JVI Journals.ASM.org

p130Cas Scaffolds the Signalosome To Direct Adaptor-Effector Cross Talk during Kaposi's Sarcoma-Associated Herpesvirus Trafficking in Human Microvascular Dermal Endothelial Cells

Chirosree Bandyopadhyay, Mohanan Valiya Veettil, Sujoy Dutta, Bala Chandran

H. M. Bligh Cancer Research Laboratories, Department of Microbiology and Immunology, Chicago Medical School, Rosalind Franklin University of Medicine and Science, North Chicago, Illinois, USA

ABSTRACT

Kaposi's sarcoma-associated herpesvirus (KSHV) interacts with cell surface receptors, such as heparan sulfate, integrins (α3β1, αVβ3, and αVβ5), and EphrinA2 (EphA2), and activates focal adhesion kinase (FAK), Src, phosphoinositol 3-kinase (PI3-K), c-Cbl, and RhoA GTPase signal molecules early during lipid raft (LR)-dependent productive macropinocytic entry into human dermal microvascular endothelial cells. Our recent studies have identified CIB1 as a signal amplifier facilitating EphA2 phosphorylation and subsequent cytoskeletal cross talk during KSHV macropinocytosis. Although CIB1 lacks an enzymatic activity and traditional adaptor domain or known interacting sequence, it associated with the KSHV entry signal complex and the CIB1-KSHV association was sustained over 30 min postinfection. To identify factors scaffolding the EphA2-CIB1 signal axis, the role of major cellular scaffold protein p130Cas (Crk-associated substrate of Src) was investigated. Inhibitor and small interfering RNA (siRNA) studies demonstrated that KSHV induced p130Cas in an EphA2-, CIB1-, and Src-dependent manner. p130Cas and Crk were associated with KSHV, LRs, EphA2, and CIB1 early during infection. Live-cell microscopy and biochemical studies demonstrated that p130Cas knockdown did not affect KSHV entry but significantly reduced productive nuclear trafficking of viral DNA and routed KSHV to lysosomal degradation. p130Cas aided in scaffolding adaptor Crk to downstream guanine nucleotide exchange factor phospho-C3G possibly to coordinate GTPase signaling during KSHV trafficking. Collectively, these studies demonstrate that p130Cas acts as a bridging molecule between the KSHV-induced entry signal complex and the downstream trafficking signalosome in endothelial cells and suggest that simultaneous targeting of KSHV entry receptors with p130Cas would be an attractive potential avenue for therapeutic intervention in KSHV infection.

IMPORTANCE

Eukaryotic cell adaptor molecules, without any intrinsic enzymatic activity, are well known to allow a great diversity of specific and coordinated protein-protein interactions imparting signal amplification to different networks for physiological and pathological signaling. They are involved in integrating signals from growth factors, extracellular matrix molecules, bacterial pathogens, and apoptotic cells. The present study identifies human microvascular dermal endothelial (HMVEC-d) cellular scaffold protein p130Cas (Crk-associated substrate) as a platform to promote Kaposi's sarcoma-associated herpesvirus (KSHV) trafficking. Early during KSHV *de novo* infection, p130Cas associates with lipid rafts and scaffolds EphrinA2 (EphA2)-associated critical adaptor members to downstream effector molecules, promoting successful nuclear delivery of the KSHV genome. Hence, simultaneous targeting of the receptor EphA2 and scaffolding action of p130Cas can potentially uncouple the signal cross talk of the KSHV entry-associated upstream signal complex from the immediate downstream trafficking-associated signalosome, consequently routing KSHV toward lysosomal degradation and eventually blocking KSHV infection and associated malignancies.

Kaposi's sarcoma-associated herpesvirus (KSHV) is etiologically linked with Kaposi's sarcoma (KS), primary effusion lymphoma (PEL), and multicentric Castleman's disease (MCD) (1–3). *In vitro*, KSHV infects several cell types by utilizing different combinations of host cell surface receptor molecules and consequently activates the associated signal pathways to facilitate its entry (4, 5). KSHV hijacks cellular endocytic machinery for its internalization in human endothelial cells, fibroblasts, B cells, and monocytes while inducing actin-dependent macropinocytosis to enter into human microvascular dermal endothelial (HMVEC-d) cells and umbilical vein endothelial (HUVEC) cells (6–12). KSHV primary infection into adherent target cells is a complex dynamic multistep process involving overlapping phases of virus attachment with multiple cell surface receptor molecules, activation of the host's preexisting cytosolic signal molecules, subsequent internalization, release of viral capsid, and cytosolic penetration toward the nucleus via motor protein cargo guided by the acetylated thickened bundles of microtubules (4).

The present study is concentrated on HMVEC-d cells, the natural *in vivo* target cells of KSHV infection. In HMVEC-d cells, KSHV initially attaches to cell surface heparan sulfate (HS) and

Received 11 June 2014 **Accepted** 17 September 2014
Published ahead of print 24 September 2014
Editor: R. M. Longnecker
Address correspondence to Bala Chandran, bala.chandran@rosalindfranklin.edu.
Supplemental material for this article may be found at http://dx.doi.org/10.1128/JVI.01674-14.

doi:10.1128/JVI.01674-14

subsequently to its entry-associated integrin receptors α3β1, αVβ3, and αVβ5 in the nonlipid raft (NLR) region of the plasma membrane. Multiple receptor engagement by KSHV results in clustering of the host's induced preexisting signaling molecules such as focal adhesion kinase (FAK), Src, phosphoinositol 3-kinase (PI3-K), c-Cbl, Rho-GTPases (RhoA, Rac, and Cdc-42), diaphanous-2, Ezrin, and other downstream effectors, all of which lead into actin rearrangement and consequently KSHV entry (13–18). Activated E3 ubiquitin ligase c-Cbl monoubiquitinates α3β1 and αVβ3 integrins, resulting in the rapid lateral translocation of virus-bound integrins into the plasma membrane lipid raft (LR) region (6). KSHV induces the LR translocation of integrins to associate and to activate LR-associated entry receptor EphrinA2 (EphA2), resulting in enhancement of EphA2 kinase action that amplifies the downstream signals (7, 19, 20). KSHV also simultaneously induced the LR translocation of calcium and integrin-binding protein 1 (CIB1) to aid in EphA2-initiated signal amplification (9). CIB1 sustains EphA2 phosphorylation and simultaneously associates with Src, c-Cbl, PI3-K, alpha-actinin 4, and myosin IIA to enhance EphA2 cross talk with the cytoskeleton to recruit macropinosome complex formation, thereby regulating productive KSHV trafficking toward the nucleus of infected HMVEC-d cells. In contrast, NLR-localized KSHV-bound αVβ5 integrins are polyubiquitinated by c-Cbl and directed to the clathrin-mediated noninfectious lysosomal pathway (21). While the process of KSHV entry-associated receptor-signal complex segregation localized to the plasma membrane LR is well characterized, the mechanistic details of postentry trafficking stages routing the cargo to infectious versus noninfectious pathways remain unknown.

Actin modulation, macropinosome assembly, closure, and trafficking are highly variable steps depending on cellular systems and the purpose of the physiological or pathological processes involved (22–30). KSHV infection induces clustering of multiple cell surface receptors and associated cytosolic signal molecules that are mostly kinases possessing canonical SH2 and SH3 adaptor domains or the noncanonical adaptor CIB1 capable of indirect association with cellular adaptors early during its entry into HMVEC-d cells (9). Host cell signal molecules are assembled in a sequential manner to the plasma membrane. Facts such as rapid KSHV entry into the target cells with virus particles sorted into Rab5-positive macropinocytic vesicles within 10 min postinfection (p.i.) and sustained activation of virus-associated signal molecules for 30 min p.i. suggest that KSHV possibly subverts host functions by spatiotemporal integration of signal adaptors during entry as well as during downstream postentry stages of infection. Hence, we explored here the identities of the potential cellular adaptor molecules capable of multiadaptor scaffold complex formation downstream to the EphA2-CIB1-c-Cbl axis and transmitting feed-forward signals during subsequent stages of KSHV entry that include macropinosome trafficking and nuclear delivery of the KSHV genome.

It was known that EphA2 associates with scaffold p130Cas (31) and that c-Cbl interacts with p130Cas immediate downstream adaptor Crk to regulate cytoskeletal rearrangement and/or endocytosis of different receptor molecules under different physiological or pathological scenarios such as intracellular evasion by pathogenic bacteria (32–34). Although a study briefly implicated p130Cas in adenovirus entry, the mechanism was not investigated (35–37). Similarly, whether simultaneous cross talk between p130Cas and Crk occurs and whether such interactions result in the recruitment of signal molecules in response to KSHV entry by macropinocytosis or in any viral entry were unknown.

p130Cas or breast cancer anti-estrogen resistance 1 (BCAR1), a 130-kDa docking protein (38, 39) lacking enzymatic or transcriptional activity, possesses multiple protein-protein interaction domains and associates with multiple adaptor-effector complexes upon substrate domain (SD) phosphorylation. Phosphorylation of the p130Cas Y-x-x-P motif is regulated by many growth factors and hormones in a Src-dependent manner (40). The most critical interaction is with members of the Crk adaptor protein, for which the Cas family is named (Crk-associated substrate of Src) (41). Like p130Cas, Crk also lacks enzymatic activity and Crk signaling is dependent on extracellular stimulation leading into the binding of Crk SH2 domains to target p-Tyr proteins (42, 43). Subsequently, the Crk SH3N domain constitutively interacts with downstream effector guanine nucleotide exchange factors (GEFs) such as Dock or C3G to activate Rho or Rap family GTPases (44). Major functions of p130Cas in physiological signaling include cell motility, survival, and proliferation. Similarly to p130Cas, downstream Crk is shown to coordinate a diverse array of cellular signaling from cell adhesion, migration, proliferation, and transcription factor-mediated gene expression, as well as phagocytosis and endocytosis in apoptotic cells (41, 45, 46). p130Cas along with Crk, or with other downstream effectors, has been reported to function in several human malignancies (38, 39, 47). However, p130Cas and Crk signaling during *de novo* infection of an oncogenic DNA virus has not been studied before. Therefore, we hypothesized that p130Cas and Crk cross talk could be crucial in coupling the KSHV entry-associated signal complex to the postentry trafficking-associated signalosome.

In this study conducted to test this hypothesis, we demonstrate that early during KSHV infection of HMVEC-d cells, p130Cas associates with cellular phosphoproteins, membrane LRs, entry receptor EphA2, entry-associated adaptor c-Cbl, and downstream adaptor Crk-effector GEF C3G and regulates KSHV productive trafficking to the nucleus. p130Cas knockdown did not affect KSHV binding or entry and, in contrast, significantly blocked the nuclear delivery of viral genome by routing KSHV to lysosomal degradation, possibly due to a reduction in Crk-C3G cross talk. These results discovered a previously unknown unique role of p130Cas as a regulator of macropinosome trafficking during pathogen infection and virus-associated cargo trafficking.

MATERIALS AND METHODS

Cells and virus. Primary HMVEC-d cells (CC-2543; Clonetics, Walkersville, MD) were grown in endothelial cell basal medium 2 (EBM2; Clonetics). KSHV carrying BCBL-1 cells was grown in RPMI with 10% total bovine serum and 1% penicillin-streptomycin antibiotic solution (48). Induction of the KSHV lytic cycle in BCBL-1 cells by tetradecanoyl phorbol acetate (TPA) (20 ng/ml), supernatant collection, and virus purification procedures were described previously (48). DNA from purified KSHV was extracted and quantitated by real-time DNA-PCR using primers amplifying the KSHV ORF73 gene as described previously (49). The same batch of purified KSHV was used for all sets of experiments.

DiI-labeled KSHV. The lipophilic carbocyanine dye DiI-1,1′-dioctadecyl-3,3,3′,3′-tetramethylindocarbocyanine perchlorate ($DiIC_{18}3$) was used to label KSHV particles according to previously established methods (6, 9, 50). Briefly, 200 μl of 1 mg/ml purified KSHV in TNE-30% sucrose buffer (TNE buffer: 0.01 M Tris-HCl, pH 7.4, 0.15 M NaCl, 0.05% EDTA) was incubated with 25 mM DiI in dimethyl sulfoxide (DMSO) for 2 h at

room temperature (RT) with gentle mixing. To remove the unbound dye, a step 10%, 30%, and 55% (wt/vol) sucrose density gradient was used. The DiI-labeled KSHV was layered on top of the 10% sucrose cushion and centrifuged at 55,000 × *g* for 90 min at 4°C. The labeled virus was collected from the top of the 55% sucrose layer and passed through a 0.22-μm filter prior to use.

Antibodies and reagents. Mouse monoclonal anti-KSHV LANA-1 and rabbit anti-gB (UK-218) antibodies were raised in our laboratory (17, 51–53). Rabbit anti-phospho-EphA2, EphA2, phospho-Src, Src, and phospho-p130Cas antibodies were from Cell Signaling Technology, Danvers, MA. Rabbit anti-CIB1 antibody was from Protein Tech, Chicago, IL. Rabbit anti-caveolin-1 and mouse anti-β-actin and tubulin antibodies were from Sigma-Aldrich, St. Louis, MO. Mouse anti-p130Cas, Crk, and c-Cbl antibodies were from BD Biosciences, San Diego, CA. Rabbit anti-transferrin and goat anti-flotillin-1 antibodies were from Abcam, Boston, MA. Rabbit phospho-C3G antibodies were from Santa Cruz Biotechnology Inc., Santa Cruz, CA. Anti-mouse and anti-rabbit IgG antibodies linked to horseradish peroxidase (HRP) were from KPL Inc., Gaithersburg, MD. 4′,6-Diamidino-2-phenylindole (DAPI), Alexa 488-conjugated LysoTracker, Alexa 594 or 488 anti-rabbit or anti-mouse, and Alexa 633 anti-mouse secondary antibodies were from Molecular Probes, Invitrogen. Cell-Light green fluorescent proteins (GFPs) (green fluorescent protein labeling reagents for early endosome, late endosome, and lysosome) were from Molecular Probes, Invitrogen. Protein G-Sepharose CL-4B was from Amersham Pharmacia Biotech, Piscataway, NJ.

Immunofluorescence microscopy. HMVEC-d cells were grown in eight-well chamber slides (Nalge Nunc International, Naperville, IL). Mock- or KSHV-infected cells were fixed with 4% paraformaldehyde (PFA) for 15 min at room temperature followed by permeabilization with 0.2% Triton X-100 for 5 min and blocked with Image-iTFX signal enhancer (Invitrogen) for 15 min. The cells were then stained with specific primary antibodies and corresponding species-specific fluorescent dye-conjugated secondary antibodies. Cells were imaged with a Nikon fluorescence microscope equipped with a MetaMorph digital imaging system.

For confocal analysis, an Olympus FV10i microscope was used for imaging, and signal intensity line scan analysis was performed on the enlarged regions of colocalization using Fluoview1000 (Olympus) software.

Western blotting. Cells were lysed in RIPA buffer (15 mM NaCl, 1 mM $MgCl_2$, 1 mM $MnCl_2$, 2 mM phenylmethylsulfonyl fluoride, and protease inhibitor mixture [Sigma]), sonicated, and centrifuged at 10,000 rpm at 4°C for 10 min. Protein concentrations were estimated with the bicinchoninic acid (BCA) protein assay reagent (Pierce, Rockford, IL). Equal concentrations of proteins were separated on SDS-PAGE, transferred to nitrocellulose, and probed with the indicated specific primary antibodies followed by incubation with species-specific horseradish peroxidase (HRP)-conjugated secondary antibody and chemiluminescence-based detection of immunoreactive protein bands (Pierce) according to the manufacturer's protocol. The bands were scanned using the FluorChem FC2 and Alpha-Imager Systems (Alpha Innotech Corporation, San Leandro, CA) and quantified with ImageJ software.

Immunoprecipitation (IP). Cells were lysed in lysis buffer (25 mM Tris-HCl, pH 7.5, 150 mM NaCl, 1% NP-40, 2 mM EDTA, 10% glycerol, and protease inhibitor mixture) sonicated, and centrifuged at 10,000 rpm at 4°C for 10 min. Two hundred micrograms of cell lysates was incubated overnight with immunoprecipitating antibody at 4°C, and the resulting immune complexes were captured by protein G-Sepharose and analyzed by Western blotting assays, using specific detection antibodies.

PLA. The proximity ligation assay (PLA) was performed using the DuoLink *in situ* starter kit and PLA reagents (Sigma-Aldrich) to detect protein-protein interactions using fluorescence microscopy according to the manufacturer's protocol (54, 55). Briefly, HMVEC-d cells were cultured in eight-well chamber slides either mock or KSHV infected (20 DNA copies/cell), fixed in 4% PFA for 15 min at room temperature, and blocked with DuoLink blocking buffer for 30 min at 37°C. Cells were then incubated with primary antibodies diluted in DuoLink antibody diluents for 1 h, washed, and then further incubated for another 1 h at 37°C with species-specific PLA probes (Plus and Minus probes) under hybridization conditions and in the presence of 2 additional oligonucleotides to facilitate hybridization of PLA probes only if they were in close proximity (<40 nm). A ligation solution and ligase were then added to join the two hybridized oligonucleotides to form a closed circle. Lastly, a detection solution consisting of fluorescently labeled oligonucleotides was added, and the labeled oligonucleotides were hybridized to the concatemeric products. The signal was detected as a distinct fluorescent dot in the Alexa Fluor 488 or Alexa Fluor 594 channel and analyzed by fluorescence microscopy. At least 10 different cells from different fields were observed for each condition and analyzed for PLA signal intensity as a proportion of DAPI-stained cells. Post-background-corrected specific PLA dot signal intensity averages and standard deviations were measured by DuoLink software (Sigma), and obtained values were mentioned in the text.

Lipid raft extraction and characterization. Lipid rafts were extracted by the nondetergent density gradient approach according to the manufacturer's protocol for the Caveola/Raft isolation kit (Sigma) (6, 7, 9, 10, 56). Briefly, uninfected and KSHV-infected cells were lysed in mild 0.5 M sodium bicarbonate buffer (pH 11.0) (containing 500 mM sodium bicarbonate, 2 mM EDTA, 1 mM NaF, 1 mM orthovanadate, and sodium protease cocktail inhibitor) for 15 min at 4°C. Cell lysates were homogenized in a precooled Dounce homogenizer by 10 strokes followed by a 10-s sonication step. OptiPrep reagent at different concentrations was used to prepare a discontinuous density gradient of five layers at 35%, 30%, 25%, 20%, and 0% in which 2 ml of 35% OptiPrep was placed as the bottommost gradient layer of the precooled ultracentrifuge tube. Each OptiPrep gradient was layered over the other using a Pasteur pipette. The tubes were subjected to ultracentrifugation at 45,000 rpm for 4 h in a Beckman SWI 55 rotor. One-milliliter fractions were collected from the top of the ultracentrifuge tube and pooled. The purity of the lipid raft-containing fractions was characterized by the presence of caveolin-1, and nonlipid rafts were confirmed by the presence of CD-71 by dot blot analysis.

Generation of HMVEC-d cells expressing CIB1 or p130Cas shRNA. CIB1 short hairpin RNA (shRNA)-expressing HMVEC-d cells were generated as previously described (9). A pool of lentivirus shRNAs specific for human p130Cas and nonspecific control shRNA was purchased from Santa Cruz Biotechnology Inc., and sequence information on respective small interfering RNA (siRNA) targets (5′→3′ orientation) is given below. HMVEC-d cells were transduced with control lentivirus shRNA or p130Cas lentivirus shRNA according to the manufacturer's instructions and selected by puromycin hydrochloride (10 μg/ml). Sequences are as indicated. sc-43271-V, CIB1 shRNA (h) lentiviral particles, is a pool of 3 different shRNA plasmids: sc-43271-VA, hairpin sequence, GATCCGCC TTAGCTTTGAGGACTTTTCAAGAGAAAGTCCTCAAAGCTAAGG CTTTTT; corresponding siRNA sequences (sc-43271A), sense, GCCUU AGCUUUGAGGACUUtt; antisense, AAGUCCUCAAAGCUAAGGCtt; sc-43271-VB, hairpin sequence, GATCCCCAGACATCAAGTCCCATTT TCAAGAGAAATGGGACTTGATGTCTGGTTTTT; corresponding siRNA sequences (sc-43271B), sense, CCAGACAUCAAGUCCCAUUtt; antisense, AAUGGGACUUGAUGUCUGGtt; sc-43271-VC, hairpin sequence, GATC CGATGACGGAACCTTGAACATTCAAGAGATGTTCAAGGTTCCGTC ATCTTTTT; corresponding siRNA sequences (sc-43271C), sense, GAU GACGGAACCUUGAACAtt; antisense, UGUUCAAGGUUCCGUCAU Ctt. Catalogue number sc-36141-V, p130Cas shRNA (h) lentiviral particles, is a pool of 3 different shRNA plasmids: sc-36141-VA, hairpin sequence, GATCCGTGGGCATGTATGATAAGATTCAAGAGATCTTA TCATACATGCCCACTTTTT; corresponding siRNA sequences (sc-36141A), sense, GUGGGCAUGUAUGAUAAGAtt; antisense, UCUUAU CAUACAUGCCCACtt; sc-36141-VB, hairpin sequence, GATCCCACAG GACATCTATGATGTTTCAAGAGAACATCATAGATGTCCTGTGTT TTT; corresponding siRNA sequences (sc-36141B), sense, CACAGGAC AUCUAUGAUGUtt; antisense, ACAUCAUAGAUGUCCUGUGtt; sc-36141-VC, hairpin sequence, GATCCGGATGGAGGACTATGACTATT

CAAGAGATAGTCATAGTCCTCCATCCTTTTT; corresponding siRNA sequences (sc-36141C), sense, GGAUGGAGGACUAUGACUAtt; antisense, UAGUCAUAGUCCUCCAUCCtt.

RNA interference using siRNA transfection. Primary HMVEC-d cells were transfected with target siRNAs using the Neon transfection system (Invitrogen) according to the manufacturer's instructions. Briefly, subconfluent cells were harvested, washed once with 1× phosphate-buffered saline (PBS), and resuspended at a density of 1×10^7 cells/ml in resuspension buffer R (provided by the company). Ten microliters of this cell suspension was mixed with 100 pmol of siRNA and then microporated at room temperature using a single pulse of 1,350 V for 30 ms. After microporation, cells were distributed into complete medium and placed at 37°C in a humidified 5% CO_2 atmosphere. At 72 h posttransfection, cells were analyzed for knockdown efficiency by Western blotting. All siRNA oligonucleotides (siGenome SMARTpool) for specific target proteins such as EphA2, CIB1, and p130Cas and nontargeting siRNA pool 1 were purchased from Thermo Scientific, and sequence information on respective siRNA targets is given as indicated. L-003116-00-0005, on-target plus human EphA2 (1969) siRNA-SMART pool, is a pool of 4 different siRNA target sequences: J-003116-09, EphA2-target sequence, UGAAUG ACAUGCCGAUCUA; J-003116-10, EphA2-target sequence, GAAGUUC ACUACCGAGAUC; J-003116-11, EphA2-target sequence, CAAGUUCG CUGACAUCGUC; J-003116-12, EphA2-target sequence, UCACACACC CGUAUGGCAA. L-012261-02-0005, on-target plus human CIB1 (10519) siRNA-SMART pool, is a pool of 4 different siRNA target sequences: J-012261-05, CIB1-target sequence, CGGCUUAGUGCGUCUG AGA; J-012261-06, CIB1-target sequence, GAGCGAAUCUGCAGGG UCU; J-012261-07, CIB1-target sequence, CCAAAGACAGCCUUAGCUU; J-012261-08, CIB1-target sequence, UGAACUGCCUCACGGGAGA. L-020465-02-0005, on-target plus human BCAR1 or p130Cas (9564) siRNA-SMART pool, is a pool of 4 different siRNA target sequences: J-020465-07, BCAR1-target sequence, GGUCGACAGUGGUGUGUAU; J-020465-08, BCAR1-target sequence, GGCCACAGGACAUCUAUGA; J-020465-09, BCAR1-target sequence, GCAAUGCUGCCCACACAUC; J-020465-10, BCAR1-target sequence, CCAGAUGGGCAGUACGAGA.

Measurement of KSHV entry by real-time DNA-PCR. For measuring entry, HMVEC-d cells were either mock or KSHV infected (20 DNA copies per cell) at 37°C for 2 h. Cells were washed with Hanks balanced salt solution (HBSS), bound and noninternalized virus was removed by treatment with trypsin-EDTA for 5 min at 37°C (49), and DNA was extracted using a DNeasy kit. Extracted DNA was quantified by amplification of the ORF73 gene by real-time DNA-PCR. The KSHV ORF73 gene cloned in the pGEM-T vector (Promega) was used as the external standard. A standard curve was generated, and the relative copy numbers of viral DNA were calculated from the threshold cycle (C_T) value.

Measurement of KSHV nuclear delivery by real-time DNA-PCR. For measuring nuclear entry of KSHV genome, pure nuclear isolation from HMVEC-d cells was performed using a Nuclei EZ Prep nuclear isolation kit (Sigma) according to the manufacturer's instructions. Briefly, HMVEC-d cells were infected with KSHV for 2 h, washed, treated with trypsin-EDTA to remove noninternalized virus, and incubated for various times of infection. Cells were then lysed on ice for 5 min with a mild lysis buffer (Sigma), and nuclei were concentrated by centrifugation at $500 \times g$ for 5 min. Cytoskeletal components loosely bound to the nuclei were removed from the nuclear pellet by a repeat of the lysis and centrifugation procedures as described previously (57). Internalized KSHV DNA was quantitated by amplification of the ORF73 gene by real-time DNA PCR (49). The KSHV ORF73 gene cloned in the pGEM-T vector (Promega) was used for the external standard. The threshold cycle (C_T) values were used to generate the standard curve and to calculate the relative copy numbers of viral DNA in the samples. A paired *t* test was used between control and shRNA-transduced cells to obtain the *P* values for the percentage of KSHV nuclear genome delivery.

Measurement of KSHV gene expression. To quantify KSHV gene expression, shControl- and shCas-transduced HMVEC-d cells grown in eight-well chamber slides were either mock or KSHV infected (20 DNA copies per cell) for 2 h in serum-free medium and at 48 h postinfection cells were fixed, permeabilized, and stained for KSHV latent protein LANA-1. At least five different fields, each containing multiple cells, were observed and analyzed as a proportion of DAPI-stained cells. A paired *t* test was used between control- and shRNA-transduced cells to obtain the *P* values for the percent inhibition in LANA-1 positivity. KSHV gene expression was also examined in siControl- and siCas-transfected HMVEC-d cells using a similar experimental setup and quantification method.

Live-cell imaging monitoring KSHV entry. For colocalization with LysoTracker, shControl- and sh-p130Cas-transduced HMVEC-d cells were infected with DiI-KSHV (50 DNA copies/cell) in the presence of Alexa 488-conjugated LysoTracker (1:100; Invitrogen) at 37°C and tracked live for ~15 min using an Olympus FV10i-LIV confocal microscope. Confocal images of DiI-KSHV and LysoTracker in selected fields with multiple cells were captured at a regular 1-min intervals at 1,024-by-1,024 resolution using a 60× (water) objective. Live-cell images were prepared using the Fluoview1000 (Olympus) software, and intensity plot profile analysis for colocalization (*x-y-z* axis) was performed on a single cell using ImageJ software. Live-cell imaging video analyses for colocalization specs (*x-y-z-t*) were performed using the Fluoview1000 (Olympus) software. Representative background-corrected images are shown.

Expression of endosomal and lysosomal markers using baculovirus-mediated gene delivery. HMVEC-d cells were transiently transduced with Cell-Light reagent BacMam 2.0 for ~16 to 19 h according to the manufacturer's protocol (Invitrogen). Briefly, HMVEC-d cells were grown in eight-well chamber slides and approximately 1×10^4 cells were infected with BacMam 2.0 at a multiplicity of infection (MOI) of 30, and at 19 h postransduction expression of Rab5a-GFP, Rab7a-GFP, and Lamp1-GFP (early endosomal, late endosomal, and lysosomal organelle markers, respectively) was monitored and the markers were ready to be used for further experiments.

RESULTS

Scaffold protein p130Cas associates with KSHV and entry receptor EphA2 early during KSHV infection of HMVEC-d cells. Our recent studies have shown that CIB1 plays the novel role of a KSHV macropinosome-associated molecule mimicking an adaptor function in HMVEC-d cell LRs to sustain KSHV entry receptor EphA2-initiated signal amplification that is followed by macropinocytic entry and establishment of *de novo* infection (9). Our study also demonstrated that CIB1 is facilitating EphA2 and cytoskeletal cross talk, such as association with alpha-actinin-4 and myosin IIA, possibly to trigger the mechanical driving force needed for macropinosome formation and subsequent productive trafficking of KSHV. CIB1 association with virus in Rab5-positive vesicles at 10 min p.i. and its cytosolic colocalization with KSHV glycoprotein gB until 30 min p.i. strongly suggested that CIB1 also plays an important role in postentry trafficking stages (9). Since structurally CIB1 lacks classical SH2 or SH3 domains, we hypothesized that CIB1 mediates this action via major cellular scaffold protein p130Cas.

To identify the role of p130Cas in *de novo* KSHV infection in HMVEC-d cells, we first tested whether p130Cas associates with virus in endothelial cells. We performed a triple colocalization study for p130Cas, envelope-labeled KSHV or DiI-KSHV, and entry receptor EphA2 as early as 10 min p.i. Our previous studies have shown that at this time point KSHV-induced signaling events are at their maximum and internalized virus particles were associated with Rab5-positive early macropinosomes. Therefore, virus tracking was carried out at 10 min p.i. as it served as a perfect transition phase to capture events of entry as well as immediate

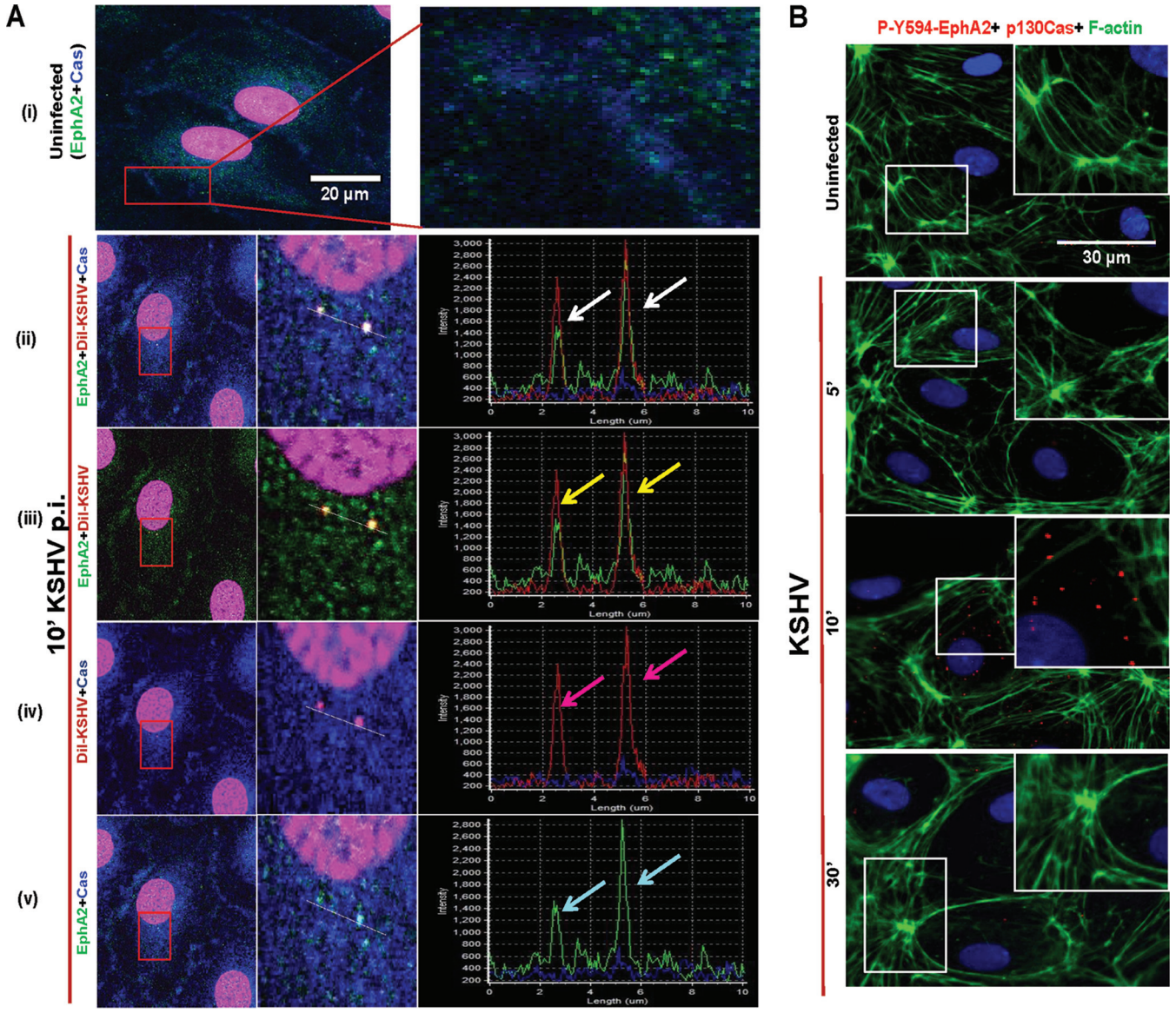

FIG 1 Confocal microscopy demonstrating the association of p130Cas with KSHV entry receptor early during *de novo* infection. (A) HMVEC-d cells were either mock or DiI-KSHV (20 DNA copies/cell) infected for 10 min at 37°C. Postwashing, cells were processed for confocal immunofluorescence using rabbit anti-EphA2 and mouse anti-p130Cas antibodies. Boxed areas in red are enlarged to the right. Representation of line scan signal intensity plots for triple staining performed on the enlarged infected-cell area (rightmost panel). Arrows indicate colocalization. Bar, 20 μm. (B) Infected cells at 5, 10, and 30 min p.i. were processed for proximity ligation assay (PLA) with rabbit anti-phospho-594-EphA2 and mouse anti-p130Cas antibodies which were subsequently costained with phalloidin-conjugated Alexa Fluor 488 and DAPI. Boxed areas in white are enlarged as an inset to the right. For PLA signals, red dots indicate the association of phospho-Y594-EphA2 and Cas molecules. Representative deconvoluted merged images are shown. Arrows indicate the colocalization. PLA signals were quantified using DuoLink tools (Sigma) as described in the text. Bar, 30 μm.

postentry trafficking stages. In uninfected cells, the colocalization between EphA2 and p130Cas was not appreciable (Fig. 1A, i, top rightmost enlarged panel). After 10 min p.i., p130Cas (blue), DiI-KSHV (red), and EphA2 (green) colocalized (white spots in Fig. 1A, ii, enlarged panel in the middle), and line scan analysis of signal intensity showed a coherent signal intensity pattern for all three stainings (Fig. 1A, ii, rightmost panel, white arrows). These observations were also validated by double colocalizations between (a) virus (red) and EphA2 (green) (yellow spots in Fig. 1A, iii, enlarged panel in the middle), (b) p130Cas (blue) and virus (red) (pink spots in Fig. 1A, iv, enlarged panel in the middle), and (c) p130Cas (blue) and EphA2 (green) (cyan spots in Fig. 1A, v, enlarged panel in the middle), respectively. Signal intensity line scan analysis and synchronous peak intensity for the respective staining also demonstrated the colocalizations between virus, EphA2, and p130Cas (colored arrows in Fig. 1A, iii, iv, and v, rightmost panel).

Proximity ligation assay (PLA) detects the association of p130Cas with pEphA2 early during KSHV infection of HMVEC-d cells. In the results shown in Fig. 1A, we observed that p130Cas associated appreciably with EphA2 only at spots where virus staining was observed. This suggested the possibility that

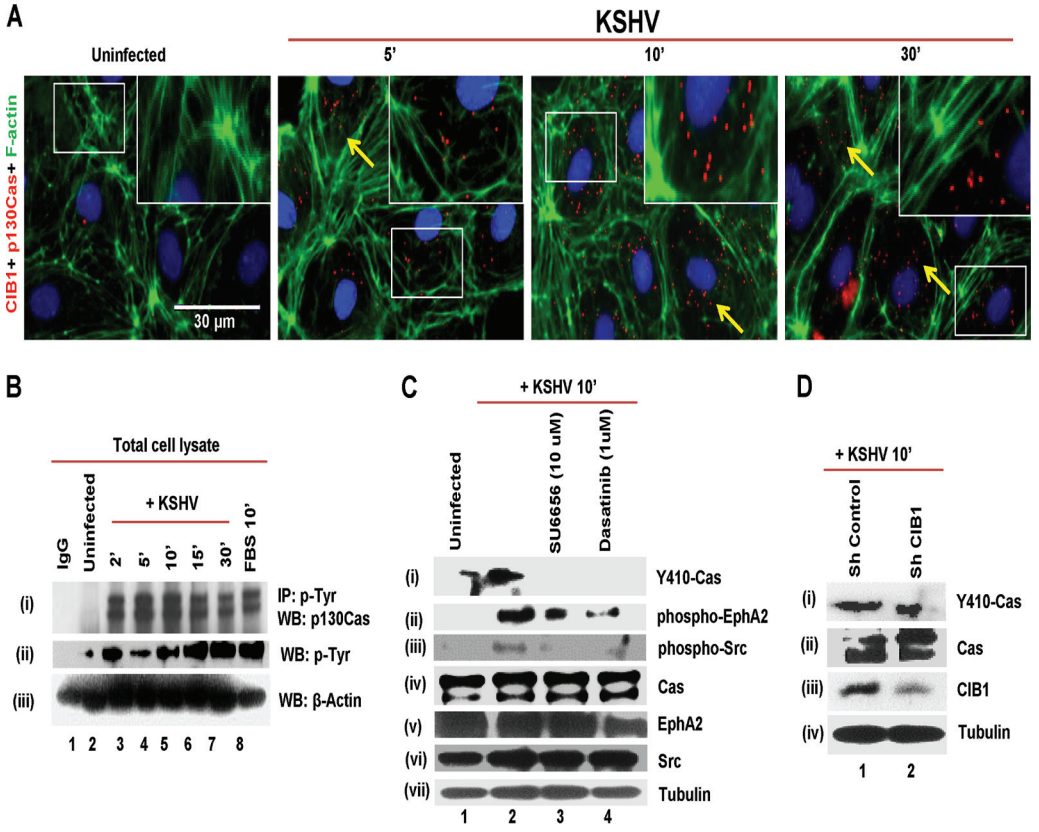

FIG 2 Demonstration of p130Cas activation during *de novo* KSHV infection of endothelial cells. (A) HMVEC-d cells were mock or KSHV infected (20 DNA copies/cell) for the indicated time points. Cells were fixed and processed for proximity ligation assay (PLA) using mouse anti-p130Cas and rabbit anti-CIB1 antibodies and costained with Alexa Fluor 488-conjugated phalloidin and DAPI. Boxed areas in white are enlarged as an inset to the right. For PLA signals, red dots indicate the association of p130Cas and CIB1 molecules. Representative deconvoluted merged images are shown. Arrows indicate the colocalization. PLA signals were quantified using DuoLink tools (Sigma) as described in the text. Bar, 30 μm. (B) HMVEC-d cells were serum starved for 8 h and infected with KSHV for the indicated time points, and lysates were immunoprecipitated with antiphosphotyrosine antibody and subjected to Western blotting (WB) with anti-p130Cas and anti-p-Tyr antibodies. Beta-actin from whole-cell lysate was used as a loading control. (C) Serum-starved (8 h) HMVEC-d cells were left untreated or SU6656 or dasatinib treated for 1 h at 37°C, infected with KSHV (20 DNA copies/cell) for 10 min, and subjected to Western blotting with anti-phospho-p130Cas, anti-phospho-EphA2, and anti-phospho-Src antibodies. Blots were stripped and reprobed for the respective total proteins and tubulin. (D) Control or CIB1 shRNA-treated cells were serum starved (8 h), infected with KSHV (20 DNA copies/cell) for 10 min, and subjected to Western blotting with anti-phospho-p130Cas antibodies. Blots were stripped and reprobed for total p130Cas, CIB1, and tubulin.

KSHV-induced Y594-phosphorylated EphA2 associates at close proximity with p130Cas at 10 min p.i. To address this, we performed a sensitive PLA between Y594 EphA2 and p130Cas in uninfected as well as in 5-, 10-, and 30-min-post-KSHV-infected HMVEC-d cells. According to the principles of proximity ligation, if two molecules are in a direct proximity of ~40 nm or less, the assay will be positive, indicating the levels of association in fluorescent dots captured by immunofluorescence microscopy (see Materials and Methods for details). Both mock- and KSHV-infected cells were costained for F-actin (phalloidin in green) to understand the spatiotemporal distribution of such associations inside the cell. In uninfected HMVEC-d cells, no appreciable PLA signals (~0.4 red dots/cell) were observed, which is possibly due to very low basal levels of pEphA2 (Fig. 1B). Although at 5 min post-KSHV infection, EphA2 was previously shown to be highly phosphorylated, no appreciable PLA signal (red dot) was detected between p-Y594 EphA2 and p130Cas, which could either be due to less association or be due to indirect association outside the 40-nm cutoff for PLA sensitivity. However, a very strong cytosolic PLA signal (~8.2 dots/cell) was observed at 10 min p.i. that corroborated our findings in Fig. 1A. These p-Y594 EphA2 and p130Cas association signals were mostly abrogated and returned to basal levels by 30 min p.i., which could be due to reduction in pEphA2 activity and hence decreased association with p130Cas. Nevertheless, these results demonstrated that 10 min p.i. is an optimal time point for p130Cas and EphA2 cross talk during *de novo* KSHV infection in HMVEC-d cells (Fig. 1B).

p130Cas associates with signal amplifier CIB1 early during KSHV infection of HMVEC-d cells. Since CIB1 aids in EphA2 phosphorylation and associates with KSHV in early macropinosomes at 10 min p.i. (9)., we examined whether CIB1 associates with p130Cas and the time kinetics of association by PLA. In uninfected HMVEC-d cells, no PLA signal for p130Cas and CIB1 interaction was observed (Fig. 2A) whereas, as early as 5 min p.i., very strong PLA signals (~40 red dots/cell) indicating CIB1 associations with p130Cas were observed both at the periphery of the cell and in the cytosol and increased over time through the observed period of 30 min p.i. These results suggested that p130Cas could be the potential scaffold molecule downstream to the receptor EphA2 signal amplifier CIB1 axis early during KSHV infection.

KSHV activates p130Cas early during infection of HMVEC-d cells. PLA results of measuring the proximity of p130Cas association with p-Y594 EphA2 and CIB1 early during KSHV infection prompted us to determine whether infection induced the association of p130Cas with other cellular phosphoproteins and/or induced the p130Cas tyrosine phosphorylation. Cells mock and KSHV infected for 2, 5, 10, 15, and 30 min p.i. were immunoprecipitated with antiphosphotyrosine (4G10) and control IgG antibodies and subjected to Western blotting for p130Cas (Fig. 2B, i). In uninfected cells, moderate tyrosine phosphorylation or association of p130Cas with p-Tyr proteins was observed (Fig. 2B, i, lane 2) and no p130Cas was detected with control IgG antibodies (Fig. 2B, i, lane 1). In contrast, p130Cas phosphorylation or association with p-Tyr-proteins increased robustly by ~2.7-fold as early as 2 min p.i., which was sustained ~2.2-fold through the observed 30 min p.i. (Fig. 2B, i, lanes 3 to 7). Induction of HMVEC-d cells with 10% fetal bovine serum (FBS), used as a positive control, also resulted in ~2.3-fold increases in p130Cas association with 4G10 (Fig. 2B, i, lane 8). KSHV-induced tyrosine phosphorylation of cellular proteins at 130 kDa (molecular mass of Cas) was tested by p-Tyr Western blotting from whole-cell lysate (WCL) using 4G10 antibody (Fig. 2B, ii). Compared to uninfected cells, KSHV-infected cells at 2, 5, 10, 15, and 30 min p.i. had respective ~1.8-, 1.4-, 1.8-, 2.3-, and 2.4-fold increases in cellular tyrosine phosphorylation (Fig. 2B, ii, lanes 2 to 7). FBS also demonstrated a 2.4-fold increase in p-Tyr at 130 kDa (Fig. 2B, ii, lane 8). Western blotting for β-actin from WCL served as loading controls (Fig. 2B, iii).

It has been well established that p130Cas is highly tyrosine phosphorylated by direct interaction with Src at 15 different Y-x-x-P motifs in its substrate domain (SD), which is associated with various functions depending on the specific phosphorylation pattern and downstream effectors. For example, motility and adhesion of cells are related to p130Cas phosphorylation at Y165, Y249, and Y410 sites (58). Phosphorylation at Y410 of p130Cas serves as a good proxy for total tyrosine phosphorylation in addition to an indicator of Src involvement in this pathway (46). Our earlier studies have demonstrated that CIB1 in synergy with EphA2 augments signals from Src in the LR that transmits signals to downstream molecules (9). From our observations that KSHV induced the association of p130Cas with phospho-EphA2 and CIB1 and that p130Cas was pulled down with phospho-Tyr antibody 4G10 (Fig. 1B and 2A and B), we reasoned that KSHV could be inducing phosphorylation at Y410 of p130Cas in an EphA2- and Src-dependent manner. To test this hypothesis, we performed inhibitor studies using Src inhibitor SU6656 and EphA2 inhibitor dasatinib, which have been shown to be specific KSHV entry inhibitors in endothelial cells (7). HMVEC-d cells were either left untreated and mock infected or treated with SU6656 (10 μM) or dasatinib (1 μM) for 1 h at 37°C and infected with KSHV for 10 min followed by Western blot analysis with p-Y410-p130Cas antibody (Fig. 2C, i). In mock-treated uninfected HMVEC-d cells, some basal level of Y-410 phosphorylation was detected (Fig. 2C, i, lane 1), which increased almost ~1.8-fold at 10 min post-KSHV infection (Fig. 2C, i, lane 2). Respective treatment with SU6656 and dasatinib almost completely abolished Y410 phosphorylation in Cas (Fig. 2C, i, lanes 3 and 4). The blot was stripped and reprobed for p-Y594-EphA2 and p-Src to test the inhibitor efficiency used in the experiments. Dasatinib inhibited EphA2 phosphorylation by 2.2-fold (Fig. 2C, ii, lane 4), and as a consequence, KSHV-induced downstream Src activation was also abolished (Fig. 2C, iii, lane 4). Since SU6656 completely abrogated Src phosphorylation (Fig. 2C, iii, lane 3), KSHV-induced EphA2 and Src feedback cross talk was also compromised, which resulted in ~1.8-fold reduction in EphA2 phosphorylation (Fig. 2C, ii, lane 3). Respective blots were stripped and reprobed for total p130Cas, EphA2, and Src (Fig. 2C, iv, v, and vi). Tubulin was used as a loading control (Fig. 2C, vii). KSHV infection did not change p130Cas expression at the protein level. These results demonstrated that p130Cas is a downstream molecule of EphA2 and Src during KSHV-induced early signal pathways in HMVEC-d cells.

Activation of p130Cas is dependent on signal amplifier CIB1 during KSHV infection. Early during KSHV infection, CIB1 synergized with EphA2 to augment signals from Src in the infected cell's LR regions to transmit signals to the downstream molecules (9). To determine whether p130Cas Y410 phosphorylation is dependent on KSHV-mediated CIB1-EphA2 activation, we tested whether KSHV could induce p130Cas Y410 phosphorylation in shCIB1-transduced HMVEC-d cells. CIB1 shRNA-expressing HMVEC-d cells were generated as previously described (9), and >1.5-fold inhibition in CIB1 expression was achieved (Fig. 2D, iii, lanes 1 and 2). Both control and CIB1 shRNA-treated HMVEC-d cells were KSHV infected for 10 min and subjected to Western blotting for phospho-Y410-p130Cas. Control shRNA did not affect p130Cas activation at Y410. In contrast, KSHV infection reduced p130Cas phosphorylation by 1.5-fold (Fig. 2D, i) in shCIB1 HMVEC-d cells, which was consistent with the levels of CIB1 knockdown in those cells. CIB1 knockdown did not change p130Cas expression at the protein level (Fig. 2D, ii). Tubulin was used as a loading control (Fig. 2D, iv). In parallel to inhibitors and shRNA studies, we also monitored the effect of EphA2 and CIB1 respective siRNAs on KSHV-induced Y410-Cas phosphorylation in HMVEC-d cells. p130Cas, CIB1, and EphA2 were knocked down at the protein level using respective siRNAs (see Materials and Methods for details) and at 72 h posttransfection tested by Western blotting using respective protein-specific antibodies. Compared to siControl HMVEC-d cells, siCas, siCIB1, and siEphA2 HMVEC-d cells had >4.6-, 2-, and 2.1-fold reductions, respectively, in Cas, CIB1, and EphA2 expression at the protein level (Fig. 3A, ii, lanes 1 and 2; A, iii, lanes 5 and 6; and A, iv, lanes 3 and 4). Y410-Cas phosphorylation was completely abolished in siCas HMVEC-d cells (Fig. 3A, i, lanes 1 and 2) and substantially reduced by >6- and 3.3-fold in siCIB1 and siEphA2 HMVEC-d cells (Fig. 3A, i, lanes 3 to 6). Cas siRNAs had no off-target effects on EphA2 and CIB1 expression (Fig. 3A, iii and iv, lanes 1 and 2). Similarly, CIB1 siRNAs did not affect Cas and EphA2 expression (Fig. 3A, ii and iii, lanes 3 and 4). Likewise, EphA2 siRNA did not alter CIB1 and Cas expression (Fig. 3A, ii and iv, lanes 5 and 6). Tubulin was used as a loading control (Fig. 3A, v, lanes 1 to 6). CIB1 siRNAs used in Fig. 3 were independent sequences against different target sequences than those for CIB1 shRNAs used in Fig. 2 (see Materials and Methods for details).

We next determined whether CIB1 associated with KSHV-induced p130Cas and the kinetics of association using the PLA method. In uninfected HMVEC-d cells, some basal-level PLA signal (~9 red dots/cell) for activated p130Cas and CIB1 association was observed (Fig. 3B), which increased substantially (~22 red dots/cell) at 10 min p.i. at the HMVEC-d cell periphery as well as in the cytosol, which was maximized (~100 red dots/cell) at 30 min p.i. These results collectively suggested that CIB1 is essential

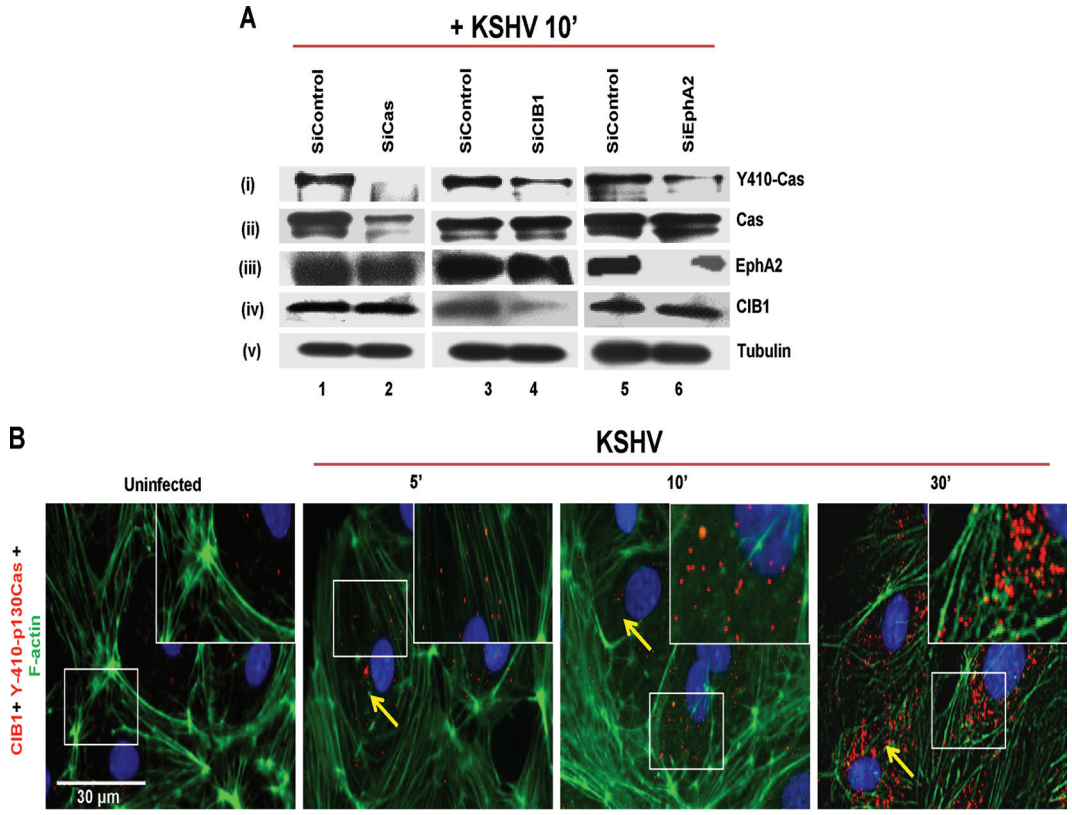

FIG 3 KSHV induced p130Cas phosphorylation in an EphA2- and CIB1-dependent manner. (A) HMVEC-d cells were transfected with siControl, siCas, siCIB1, or siEphA2 and at 72 h posttransfection were infected with KSHV (20 DNA copies/cell) for 10 min and subjected to Western blotting with anti-phospho-p130Cas antibodies. Blots were stripped and reprobed for total p130Cas, EphA2, CIB1, and tubulin. (B) HMVEC-d cells were mock or KSHV infected (20 DNA copies/cell) for the indicated time points. Cells were fixed and processed for proximity ligation assay using mouse anti-CIB1 and rabbit anti-phospho-p130Cas antibodies and costained with Alexa Fluor 488-conjugated phalloidin and DAPI, which were merged with the deconvoluted images. Boxed areas in white are enlarged as an inset to the right. For PLA signals, red dots indicate the association of phospho-Y410-p130Cas and CIB1 molecules. Representative deconvoluted images are shown. Arrows indicate colocalization. PLA signals were quantified using DuoLink tools (Sigma) as described in the text. Bar, 30 μm.

for p130Cas activation and that CIB1 and p130Cas could be coordinating together in the postentry stages of KSHV infection, such as viral trafficking.

Crk, a p130Cas immediate downstream molecule, associates with KSHV, EphA2, and signal amplifier CIB1 early during KSHV infection of HMVEC-d cells. Studies thus far strongly suggested that p130Cas is involved in KSHV-induced *de novo* signal pathways in HMVEC-d cells and KSHV-induced Y410 phosphorylation of Cas SD downstream to the EphA2-CIB1-Src signal axis. Since p130Cas SD phosphorylation is shown to induce downstream Crk-SH2 domain binding to Cas to stimulate cellular motility under physiological as well as pathological conditions (41), we next determined whether Crk associates with KSHV early during infection. In immunofluorescence studies, Crk colocalized with KSHV detected by envelope glycoprotein gB antibodies at 5 and 30 min p.i. (Fig. 4A, white arrows). Since CIB1 was previously reported to associate with virus at these time points (9), we utilized PLA to determine whether CIB1 and Crk interact during KSHV infection. In uninfected HMVEC-d cells, no appreciable PLA signal (~0.5 red dots/cell) for Crk and CIB1 association was observed (Fig. 4B). In contrast, as early as 5 min p.i., a very strong PLA signal (~6 red dots/cell) indicating CIB1 and Crk associations was observed at the HMVEC-d cell periphery as well as in the cytosol, which was robustly maximized (~30 red dots/cell) at 10 min p.i. and sustained (~10 red dots/cell) until 30 min p.i. These results clearly suggested the possibility of CIB1-p130Cas-Crk cross talk early during the postentry stage of infection and extending throughout the trafficking stages of KSHV infection.

KSHV-induced LR recruitment of p130Cas and downstream Crk. Our previous studies have demonstrated that CIB1 translocates into HMVEC-d cell LRs and associates with EphA2 at 10 min p.i. (9). Since p130Cas and Crk associated with CIB1 at 10 min p.i., we theorized that both the scaffold and adaptor molecules are recruited to the infected HMVEC-d cell LRs. To analyze p130Cas and Crk association with LRs of infected cells, we biochemically isolated LRs and NLRs from mock- and KSHV-infected HMVEC-d cells at 2, 5, 10, and 30 min p.i. by previously established methods (6, 9, 10, 55). The purity of LR and NLR fractions was initially checked by dot blot analysis for LR marker caveolin-1 and NLR marker CD-71 (data not shown). Pure fractions were pooled accordingly and examined by Western blotting assays (Fig. 5A). Caveolin-1 and CD-71 were blotted from the fractions as purity controls (Fig. 5A, iii and iv).

The scaffold p130Cas protein was minimally associated with both uninfected-cell NLRs (Fig. 5A, i, lane 1) and LRs (Fig. 5A, i, lane 1). In contrast, as early as 2 min p.i., we observed a robust association of p130Cas with infected-cell LRs which was sustained for 30 min p.i. (Fig. 5A, i, lanes 2 to 5). The adaptor Crk molecules

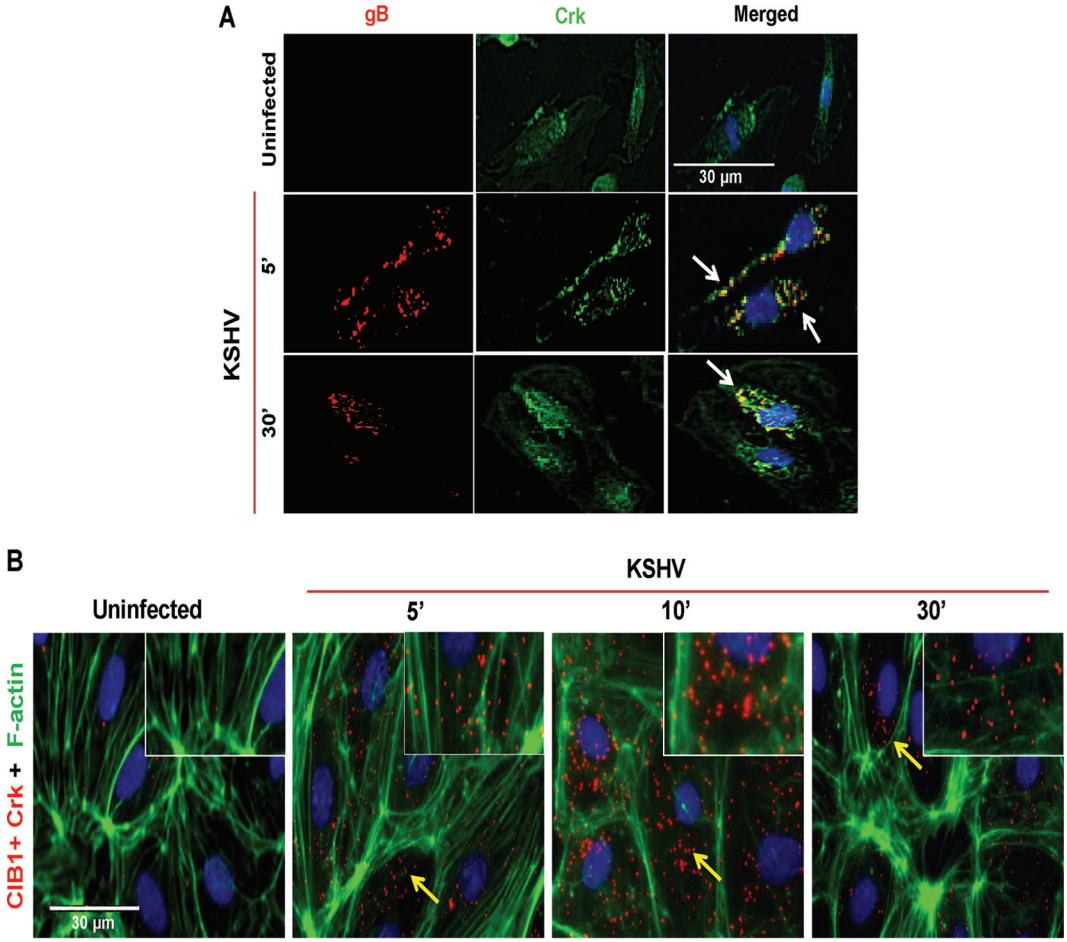

FIG 4 Colocalization of p130Cas and its downstream Crk molecules with KSHV and CIB1. (A) Uninfected HMVEC-d cells or cells infected with KSHV (20 DNA copies/cell) for 5 min and 30 min were processed for IFA, reacted with mouse anti-Crk antibodies and rabbit anti-KSHV glycoprotein gB antibodies, and costained with DAPI. Arrows indicate colocalization of Crk with virus particles at the indicated time points. Bar, 30 μm. (B) Infected cells at 5, 10, and 30 min p.i. were processed for proximity ligation analysis with mouse anti-CIB1 and rabbit anti-phospho-p130Cas antibodies and subsequently costained with Alexa Fluor 488-conjugated phalloidin and DAPI, which were merged with the deconvoluted images. Boxed areas in white are enlarged as an inset to the right. For PLA signals, red dots indicate the association of phospho-p130Cas and CIB1 molecules. Representative deconvoluted merged images are shown. Arrows indicate the colocalization. PLA signals were quantified using DuoLink tools (Sigma) as described in the text. Bar, 30 μm.

also demonstrated kinetics of LR association similar to that of upstream scaffold p130Cas molecules (Fig. 5A, ii). In immunoprecipitation (IP) reactions with anti-EphA2 antibodies, Crk was associated with EphA2 only in the infected-cell LR fractions (Fig. 5B, i, lanes 1 to 6) and not in the NLR fractions, and this association increased over time with maximal association at 10 min p.i. and decreased thereafter (Fig. 5B, i, lanes 2 to 6).

To confirm these biochemical results, HMVEC-d cells were mock or KSHV infected for 5 and 10 min, and LR association of p130Cas and Crk was examined by immunofluorescence assay (IFA) (Fig. 5C and D). In uninfected HMVEC-d cells, p130Cas (green) did not show any appreciable colocalization with LR marker flotillin-1 (red) (Fig. 5C). In contrast, as early as 5 min p.i., clustered p130Cas colocalized very strongly with LRs at the cell periphery as well as in the cytosol and the colocalization was sustained over 30 min p.i. (Fig. 5C, second and third panels, white arrow). This indicated the association of p130Cas with LRs, which probably initiates the clustering of multiple adaptor-effectors. IFA studies also revealed kinetics similar to those of p130Cas downstream Crk association with LRs (Fig. 5D), which was consistent with our biochemical data (Fig. 5A and B). However, due to clustering of signal molecules with LR, colocalization signal intensity in IFA appears stronger than biochemical data demonstrating LR translocation of adaptor molecules. Taken together, temporal enrichment of p130Cas and Crk to the LR-EphA2 signal hubs upon KSHV infection strongly suggested that p130Cas is a key scaffold molecule regulating KSHV-induced EphA2-signal induction events during *de novo* infection in HMVEC-d cells.

p130Cas assembles EphA2, c-Cbl, and Crk signal complexes early during KSHV infection of HMVEC-d cells. We next determined whether KSHV infection triggered p130Cas scaffold function and simultaneous assembly of receptor-adaptor-effector molecules early during KSHV infection. Serum-starved HMVEC-d cells were mock or KSHV infected for 5, 10, and 30 min; immunoprecipitated with anti-p130Cas antibody; and subjected to Western blotting for KSHV entry receptor EphA2, entry adaptor c-Cbl, and p130Cas downstream adaptor Crk molecule. Co-IP and PLA experimental results, summarized as a model in Fig. 6A, collectively

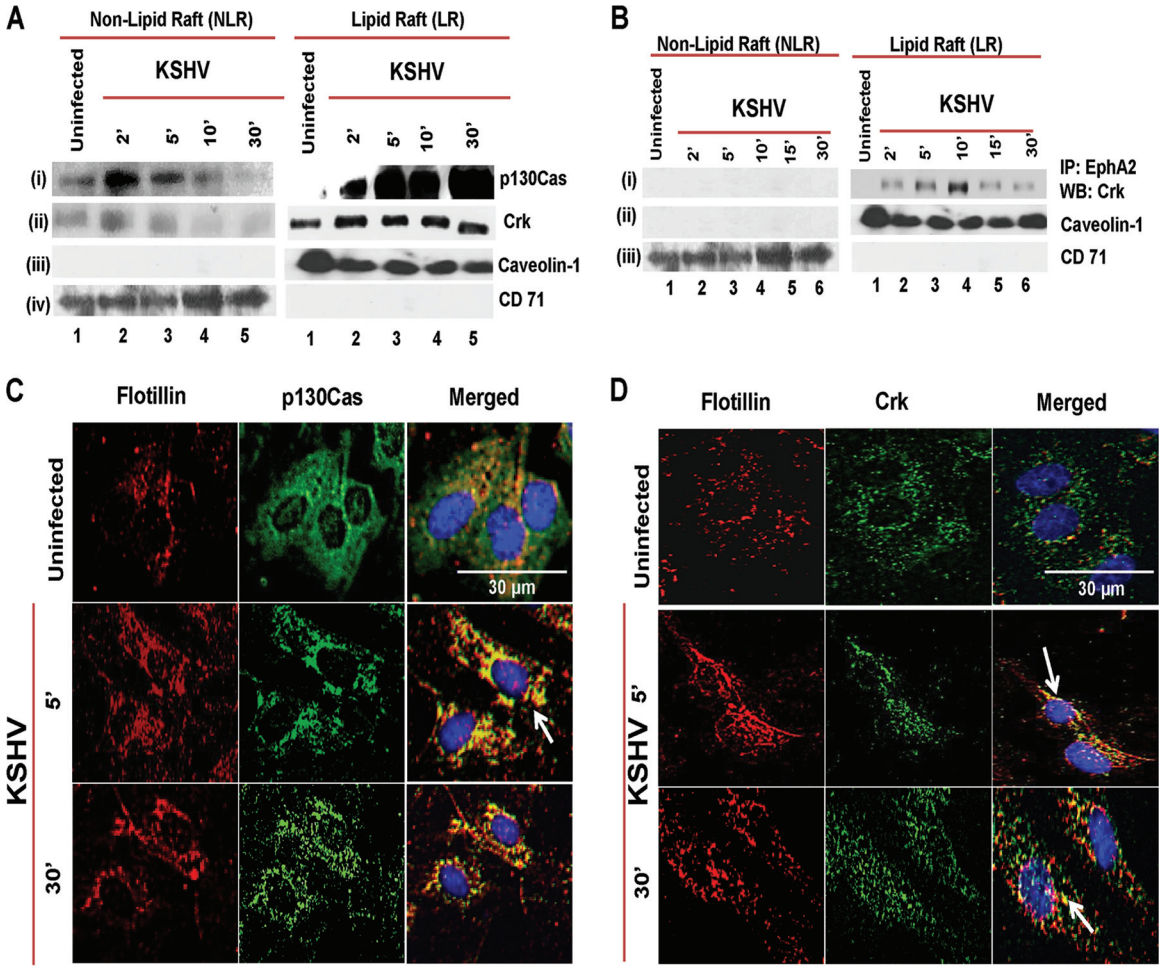

FIG 5 Association of p130Cas and its downstream Crk molecules with lipid rafts early during *de novo* KSHV infection. (A) Serum-starved (8 h) HMVEC-d cells were either mock or KSHV infected (20 DNA copies/cell) for the indicated time points. LR and NLR fractions were isolated and analyzed for p130Cas and Crk levels by Western blot assays. (B) LR and NLR fractions from the same experiment were subjected to immunoprecipitation with anti-EphA2 antibodies and subjected to Western blotting with anti-Crk antibodies. Caveolin-1 and CD71 characterize the purity of LR and non-LR fractions, respectively. (C and D) Serum-starved (8 h) HMVEC-d cells were either left uninfected or infected (20 DNA copies/cell) for the indicated time points with KSHV (20 DNA copies/cell), washed, and processed for double immunofluorescence using mouse anti-p130Cas (C) or Crk (D) and goat anti-flotillin-1 (LR marker) antibodies, followed by Alexa 594 and Alexa 488 antibodies, respectively. Representative deconvoluted immunofluorescence images are shown. Arrows indicate colocalization. Bar, 30 μm.

suggested that EphA2, CIB1, c-Cbl, p130Cas, and Crk association is enhanced temporally upon KSHV infection, perhaps to initiate a transition phase from KSHV postentry leading into KSHV trafficking, including the association of activated guanine nucleotide exchange factor C3G. Minimal or no association of p130Cas with EphA2, c-Cbl, and Crk was seen in uninfected HMVEC-d cells (Fig. 6B, i, ii, and iii, lane 1). In contrast, with KSHV infection, a robust increase in p130Cas associations with these molecules was observed that was maximized at 10 min p.i. and was detectable until 30 min p.i. (Fig. 6B, i, ii, and iii, lanes 2 to 4). The membrane was stripped and probed to check total p130Cas levels (Fig. 6B, iv).

To validate the KSHV-induced simultaneous interaction of p130Cas with signal molecules, the same experimental lysates as above were reverse co-IPed with anti-EphA2, anti-c-Cbl, and anti-Crk antibodies and subsequently subjected to Western blotting for all of these signal molecules (Fig. 6C, D, and E). Blots were stripped and reprobed for respective total protein levels of each signal molecule (Fig. 6C, D, and E). Results from EphA2 immunoprecipitation analyses indicated that upon KSHV infection EphA2 associated more robustly with Crk than with p130Cas and that both of these associations were sustained for 30 min p.i. (Fig. 6C, i and ii, lanes 2 to 4). c-Cbl immunoprecipitation analyses revealed that upon KSHV infection c-Cbl associates with EphA2 maximally at 10 min p.i. (Fig. 6D, i, lane 3) and that this association was reduced by 30 min p.i. (Fig. 6D, i, lane 4). In contrast, enhanced c-Cbl associations with p130Cas and Crk were observed upon infection and sustained for 30 min p.i. (Fig. 6D, ii and iii, lanes 2 to 4). Crk immunoprecipitation analyses revealed that KSHV induced a robust Crk association with both EphA2 and p130Cas as early as 5 min p.i., which was sustained for 30 min p.i. (Fig. 6E, i and ii, lanes 2 to 4).

C3G molecules are guanine nucleotide exchange factors, activated downstream of the p130Cas-Crk axis to influence GDP-GTP exchange directly or indirectly in a variety of downstream cellular GTPases that include the Ras, Rac, Rho, and Rap families (44). Our earlier studies have shown that early during binding and

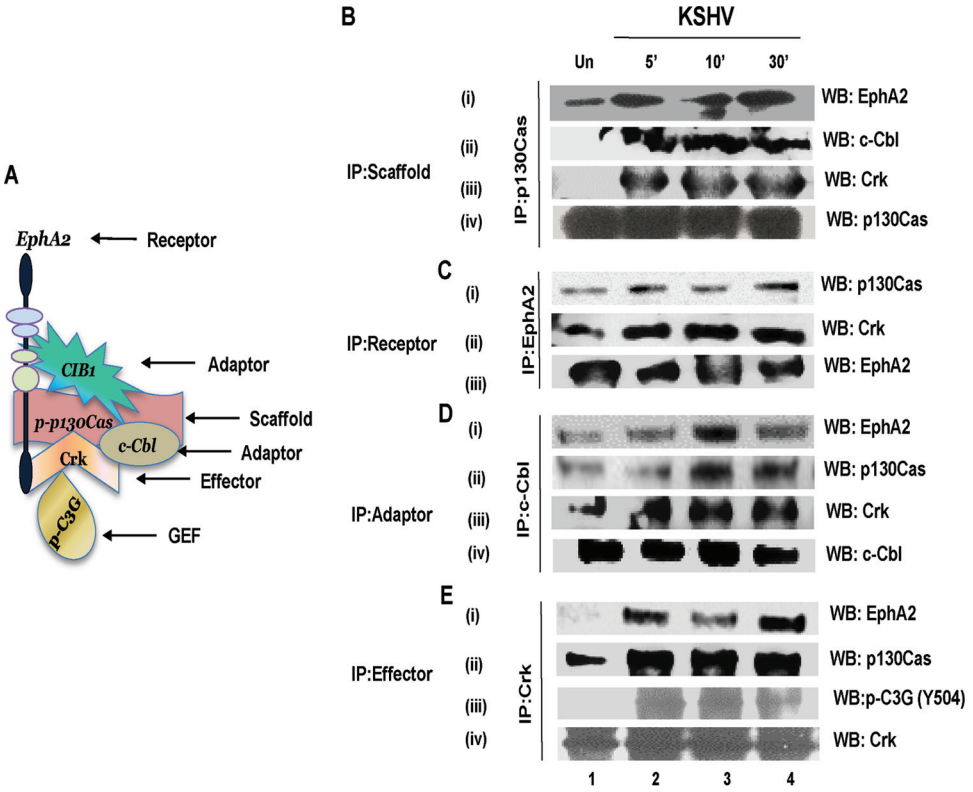

FIG 6 Association of p130Cas with KSHV-induced signalosome. (A) Model summarizing the coimmunoprecipitation and PLA experiments to portray KSHV-induced signalosome assembly. (B to E) Serum-starved (8 h) HMVEC-d cells were either mock or KSHV infected (20 DNA copies/cell) for the indicated time points; immunoprecipitated with IP antibodies for p130Cas (B), EphA2 (C), c-Cbl (D), and Crk (E); and analyzed by Western blotting (WB) for the indicated signal molecules. Blots were stripped and reprobed for respective signal molecules to detect the total levels of these molecules.

entry stages, KSHV entry induces reactive oxygen species and activates Rho-GTPase, both of which are utilized to promote cytoskeletal motility during KSHV entry and productive trafficking. We have also shown that KSHV-induced activation of RhoA was also dependent on EphA2, Src, and PI3-K (7, 14, 57). Since our co-IP studies demonstrated robust p130Cas and Crk association at 5, 10, and 30 min p.i., to determine whether the EphA2-CIB1-p130Cas-Crk signal axis is involved in KSHV-induced GTPase activation, possibly via Crk-C3G cross talk, we examined the association of p130Cas and Crk with activated effector GEF C3G. Serum-starved HMVEC-d cells were mock or KSHV infected for 5, 10, and 30 min; immunoprecipitated with anti-Crk antibody; and subjected to Western blotting for activated GEF molecule phospho-Y504-C3G. In uninfected cells, little or no association was observed between Crk and phospho-C3G (Fig. 6E, iii, lane 1). In contrast, KSHV infection induced a transient association of Crk with phospho-C3G as early as 5 min p.i., which was sustained till 30 min p.i. (Fig. 6E, iii, lanes 2 to 4).

p130Cas knockdown inhibits KSHV nuclear delivery and gene expression. To characterize the functional effects of p130Cas on KSHV infection, we used p130Cas lentivirus encoding shRNA to knock down p130Cas activity in HMVEC-d cells. p130Cas shRNA inhibited >90% of p130Cas expression as detected by Western blotting with specific anti-p130Cas antibodies (Fig. 7A). Tubulin was used as a loading control (Fig. 7A). p130Cas shRNA did not have any off-target effects on immediate upstream host cell signaling molecule Src, an important KSHV entry mediator (Fig. 7A).

To determine the effect of p130Cas shRNA on KSHV infection, control shRNA- and p130Cas shRNA-transduced HMVEC-d cells were grown in eight-well chamber slides, infected with KSHV for 48 h, and stained for KSHV latency-associated LANA-1 (ORF73) protein. In contrast to control shRNA-treated cells, in p130Cas shRNA-transduced cells we observed ~70% reduction in the characteristic nuclear LANA-1 punctate staining (Fig. 7B).

We reasoned that the decrease in KSHV gene expression could be due to a block at any of the multiple overlapping steps associated with *de novo* KSHV infection in HMVEC-d cells such as virus binding, entry, or nuclear delivery. Hence, we examined the effect of p130Cas shRNA at each of these steps. Similar levels of KSHV binding (~25,100 bound viral DNA copies) were detected in both p130Cas shRNA- and control shRNA-transduced cells (Fig. 7C), which demonstrated that p130Cas does not play a role in KSHV binding. Similarly, KSHV entry experiments also showed comparable levels of internalized viral DNA copies in both control and p130Cas shRNA-transduced cells and hence no notable decrease (~10%) in entry (Fig. 7D) as measured by real-time DNA-PCR for the KSHV ORF73 gene, which was consistent with our live-cell imaging experiment (described in Fig. 8). In contrast, compared to control shRNA-transduced cells, KSHV nuclear delivery was significantly reduced by 50% in p130Cas shRNA-transduced HMVEC-d cells as measured by real-time DNA-PCR for KSHV gene ORF73 with DNA isolated from the infected-cell nucleus (Fig. 7E). We further validated the role of p130Cas in KSHV infectivity by also using siRNAs against p130Cas (Fig. 7G to I) with different target sequences than those for shRNAs used in Fig. 7A to

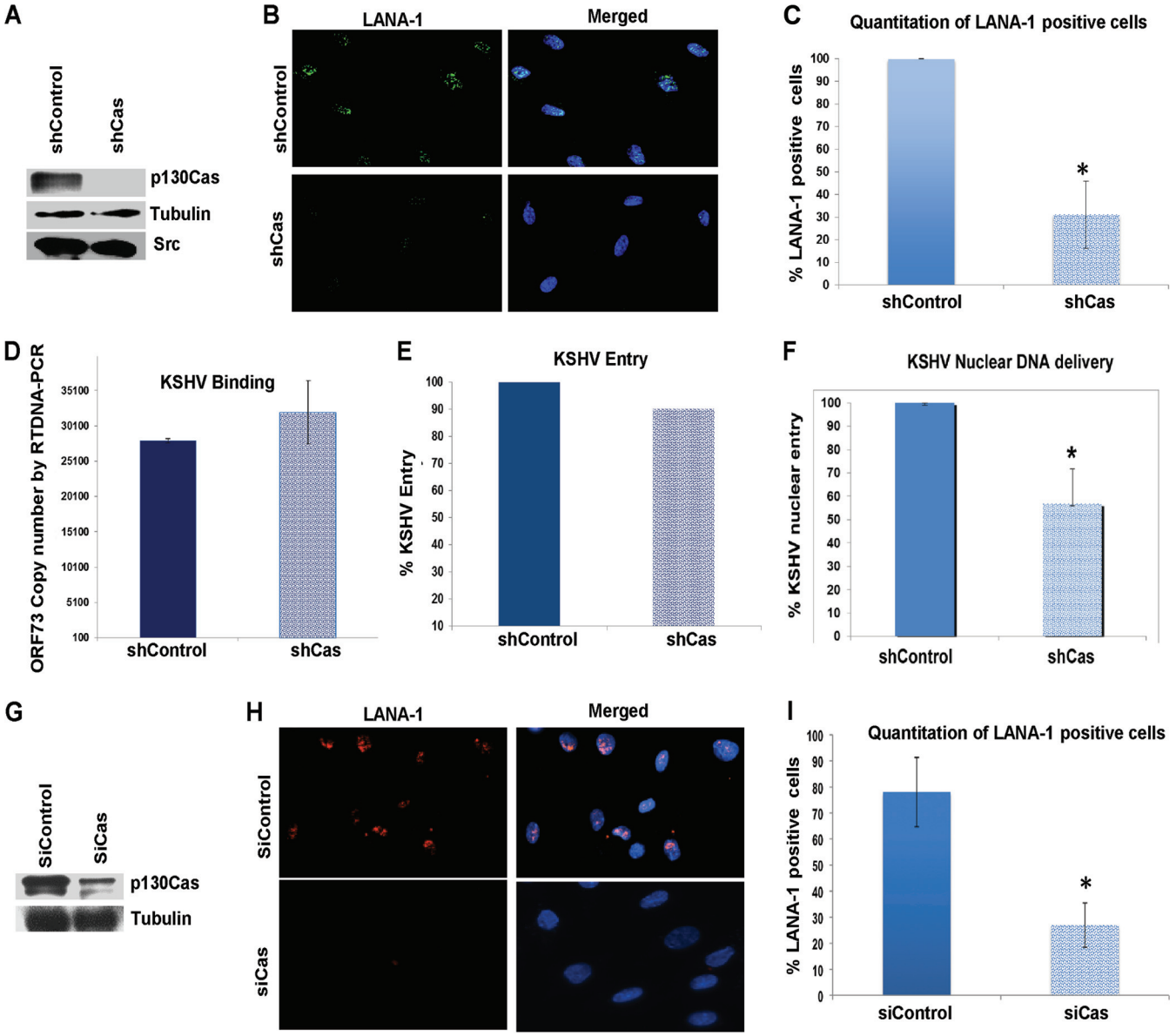

FIG 7 Effect of p130Cas shRNA on KSHV infection. (A) HMVEC-d cells were either untransduced or transduced with shControl- or sh-p130Cas-expressing lentivirus particles and selected with puromycin. Knockdown of p130Cas protein expression was examined by Western blotting for Cas (specific shRNA target), tubulin, and Src (off-target molecules). (B) Control or Cas shRNA-transduced HMVEC-d cells were mock or KSHV infected (20 DNA copies/cell) for 2 h at 37°C, washed to remove unbound viruses, and cultured for another 46 h. At 48 h p.i., cells were processed for immunofluorescence analysis using mouse anti-LANA-1 antibodies and costained with DAPI. Representative deconvoluted images are shown. (C) The percentage of cells observed positive for characteristic punctate LANA-1 staining in IFA is presented graphically. A minimum of 10 independent fields, each with at least 5 cells, were chosen. Error bars show ±standard deviations. (D and E) Untransduced, control shRNA- and Cas shRNA-transduced HMVEC-d cells were infected with KSHV (20 DNA copies/cell) for 1 h at 4°C (D) or 2 h at 37°C (E) for binding and entry experiments, respectively. Postwashing, total DNA was isolated and KSHV binding and entry were determined by real-time DNA-PCR for the KSHV ORF73 gene. Each reaction was done in triplicate, and a representative result is plotted. For binding studies, results are presented as KSHV DNA copies bound to Cas shRNA-transduced and control shRNA-transduced cells. Error bars show ±standard deviations. For entry studies, results are presented as percentage of inhibition of KSHV DNA internalization by shCas or shControl compared with infected untransduced cells. (F) Control shRNA- and Cas shRNA-transduced HMVEC-d cells were infected with KSHV (20 DNA copies/cell) for 2 h at 37°C. Postwashing, nuclei were purified from both uninfected and infected cells and DNA was isolated. Nuclear entry was determined by real-time DNA-PCR for the KSHV ORF73 gene. Each reaction was done in triplicate. Error bars show ±standard deviations. (G) HMVEC-d cells were transfected with either control siRNA or p130Cas siRNA, and at 72 h posttransfection, knockdown of p130Cas protein expression was examined by Western blotting for Cas (specific shRNA target) and tubulin. (H) Control or Cas siRNA-transfected HMVEC-d cells were mock or KSHV infected (30 DNA copies/cell) for 2 h at 37°C, washed to remove unbound viruses, and cultured for another 22 h. At 24 h p.i., cells were processed for immunofluorescence analysis using mouse anti-LANA-1 antibodies and costained with DAPI. Representative images are shown. (I) The percentage of cells observed positive for characteristic punctate LANA-1 staining in IFA is presented graphically. A minimum of 10 independent fields, each with at least 8 cells, were chosen. Error bars show ±standard deviations. *, $P < 0.05$.

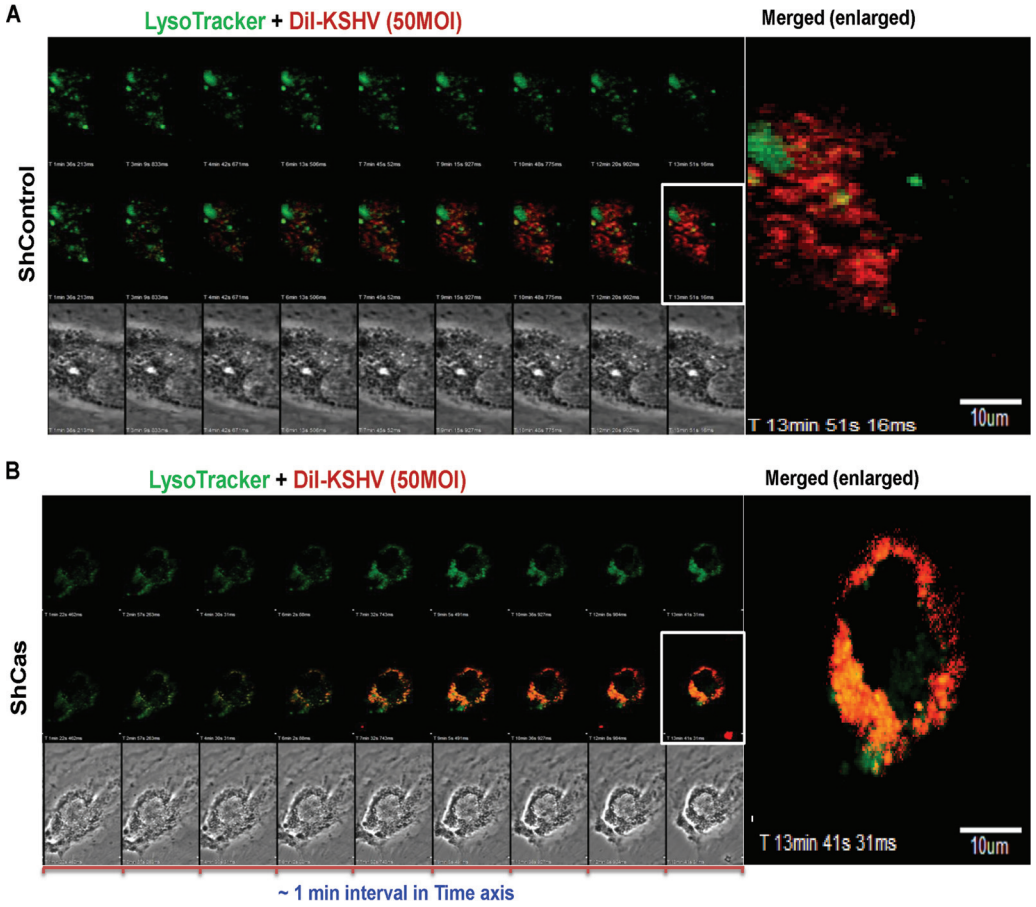

FIG 8 Effect of p130Cas shRNA on the trafficking of internalized KSHV. Control shRNA (A)- or p130Cas shRNA (B)-transduced cells were infected with DiI-KSHV (55 DNA copies/cell) and were tracked with LysoTracker (green) by live-cell microscopy for the indicated time points. Images were taken using an Olympus FV10-LIV confocal microscope with a 60× water objective. From 1 min p.i., live images were taken until ~15 min p.i., and images were background corrected using Olympus Fluoview1000. Representative images are shown. Bar, 10 μm.

F (see Materials and Methods for details). At 72 h posttransfection, p130Cas siRNAs inhibited Cas expression by >70% at the protein level (Fig. 7G). Tubulin was used as a loading control (Fig. 7H). In contrast to control siRNA-transfected HMVEC-d cells, p130Cas siRNA-transfected cells resulted in an ~61% reduction in the characteristic nuclear LANA-1 punctate staining (Fig. 7H and I). These results strongly established that p130Cas plays a functional role in KSHV primary infection in HMVEC-d cells and that p130Cas is a key signal regulatory molecule during KSHV postentry stages of infection.

p130Cas knockdown routed KSHV toward lysosomal degradation. We have earlier shown that knocking down cellular adaptor c-Cbl inhibited KSHV receptor translocation to the LR and that NLR-bound KSHV internalized via the clathrin pathway was degraded in the lysosome (6). Our previous studies also demonstrated that knocking down EphA2, the strictly LR-associated KSHV entry receptor, shut down the productive macropinocytosis pathway (7). Since p130Cas knockdown did not affect KSHV entry but inhibited productive trafficking to the nucleus and successful latent gene expression, we reasoned that although KSHV macropinocytosis is not hampered, p130Cas might be involved in macropinosome trafficking. To visualize whether knocking down p130Cas rerouted KSHV to the lysosome, we performed a live-cell coendocytosis experiment with envelope-labeled KSHV (DiI-KSHV) and LysoTracker (a basophilic tracking dye for lysosomes) in both control shRNA (Fig. 8A)- and p130Cas shRNA (Fig. 8B)-transduced HMVEC-d cells. After addition of DiI-KSHV (red) and LysoTracker (green) to the cells, the event was tracked live for 15 min (Fig. 8), frames were taken at a regular interval of 1 min, and representative images are displayed (Fig. 8).

In both control and p130Cas shRNA-transduced cells (Fig. 8A and B), KSHV infection induced membrane blebs as early as 1 min p.i. (Fig. 8A and B, differential interference contrast [DIC] images in the bottommost panels) and KSHV subsequently entered the cell. Multiple virus particles constantly induced blebs as observed by the presence of blebs throughout the entry experiment, possibly due to the high titer of KSHV (50 DNA copies/cell). Uptake levels of LysoTracker and DiI-KSHV were similar in control shRNA- and p130Cas shRNA-transduced cells. However, most of the internalized virus particles in p130Cas knockdown HMVEC-d cells colocalized with LysoTracker as analyzed by ImageJ software and displayed (see Fig. S1 in the supplemental material). Increased colocalization between LysoTracker and DiI-KSHV was also monitored by increased accumulation of colocalization specks between DiI-KSHV and lysosomal compartments over time. Signal intensities from individual channels (Ch2, red, upon Ch1, green)

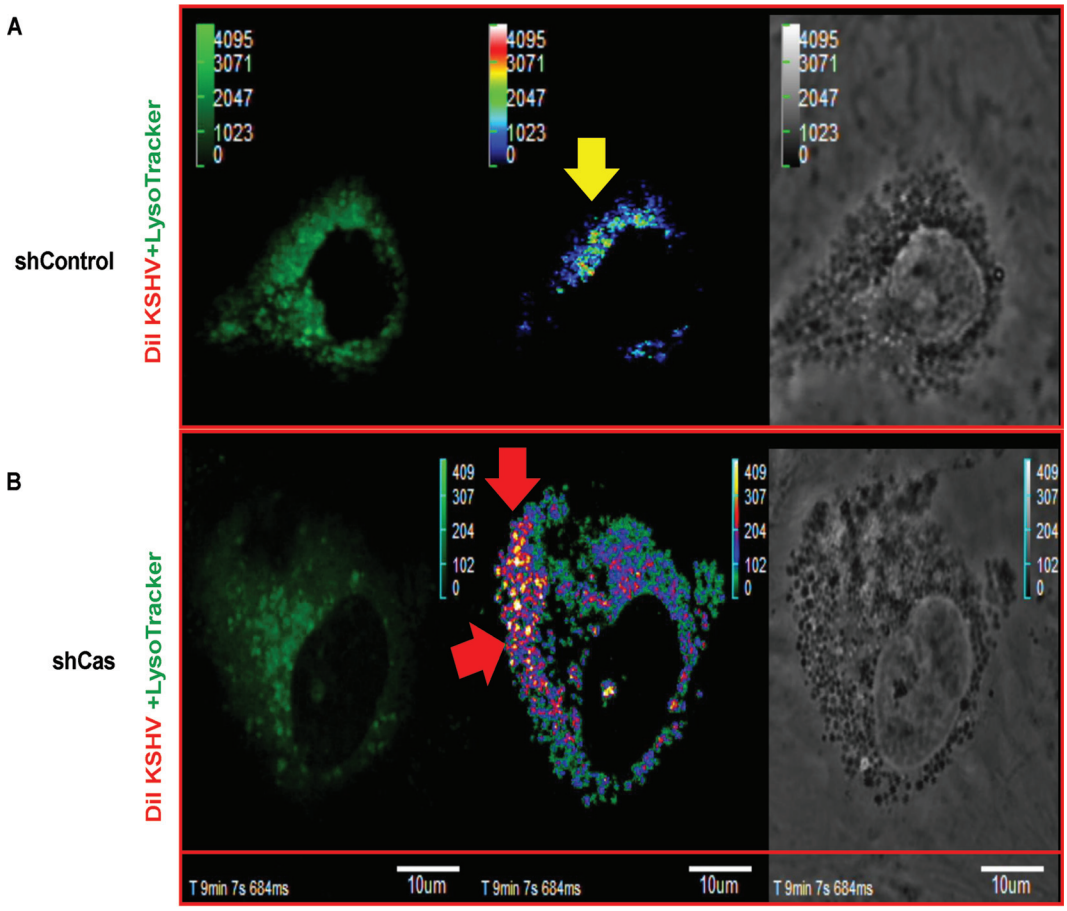

FIG 9 Overview of DiI-KSHV and LysoTracker colocalization specks during coendocytosis in shControl versus shCas HMVEC-d cells. The experiment was performed as described in the legend to Fig. 8. Signal intensity for LysoTracker (Ch1; green) and signal intensity for DiI-KSHV (Ch2; red) were background corrected and overlapped (*x-y-z-t* axis) using Olympus Fluoview1000 software. Analyses are displayed as accumulated colocalization intensity (Ch2 on Ch1) in the form of specks (on an average colocalization intensity scale ranging from 0 to 4,029 arbitrary units) at ~10 min p.i. of control (A) or p130Cas shRNA (B)-transduced HMVEC-d cells. Bar, 10 μm. Respective videos for colocalization specks (*x-y-z-t* axis) were prepared using Olympus Fluoview1000 and are included in Movies S1 and S2 in the supplemental material. Yellow and red arrows indicate DiI-KSHV colocalization with LysoTracker in shControl and shCas cells, respectively.

were merged to represent colocalization specks on an arbitrary unit (AU) scale for colocalization (accumulation of virus in lysosomal compartments) with intensity ranging from 0 to 4,095 AU. Images (Fig. 9) were generated using Fluoview1000 software. In control shRNA-transduced HMVEC-d cells, colocalization speck intensities at ~10 min p.i. were low (Fig. 9A) compared to those in p130Cas shRNA-transduced HMVEC-d cells (Fig. 9B), which strongly corroborated previous methods of live-cell imaging analysis data (Fig. 8). Live-cell imaging movies for colocalization speck analysis are included in the supplemental material (see Movies S1 and S2). In control shRNA-transduced HMVEC-d cells, lysosomes are less active, and as previously published (6, 7), only a very few DiI-KSHV particles entered by the clathrin-mediated nonproductive infection pathway, demonstrating a minimal colocalization with lysosomes. A significantly higher level of perinuclear staining of KSHV was observed in shCas HMVEC-d cells than in control shRNA-transduced HMVEC-d cells (Fig. 8B and 9B). The reason behind this observation is due to characteristic perinuclear trans-Golgi staining of active lysosomes (59–64). These results demonstrated that the reduction of KSHV nuclear viral DNA entry and gene expression in sh-p130Cas HMVEC-d cells is due to virus entering the cell and being directed to the lysosomal noninfectious pathway. These data strongly corroborated other findings in the present study and established that the p130Cas signal complex plays major roles in proper KSHV postentry trafficking events resulting in viral DNA entry into the nucleus.

Mechanism of p130Cas action in routing proper KSHV trafficking. To understand the mechanism of p130Cas action in KSHV cargo trafficking, we first tested the p130Cas downstream signal molecule cross talk events. Our present findings demonstrated Cas downstream Crk and effector C3G cross talk during KSHV *de novo* infection in HMVEC-d cells (Fig. 6E, iii, lanes 2 to 4). Therefore, we hypothesized that p130Cas knockdown may disrupt the association between Crk and C3G and subsequently affect cellular GTPase signaling to block KSHV trafficking. To address this, we utilized the PLA method. Control and p130Cas shRNA-transduced cells were infected with KSHV and at 5, 10, and 30 min p.i. processed for PLA with Crk- and phospho-Y504-C3G-specific antibodies. Control shRNA-treated HMVEC-d cells demonstrated an increase in PLA signals (green dots) for phospho-Y504-C3G and Crk association at 10 and 30 min after infection with KSHV compared to uninfected shControl cells (Fig. 10A). These

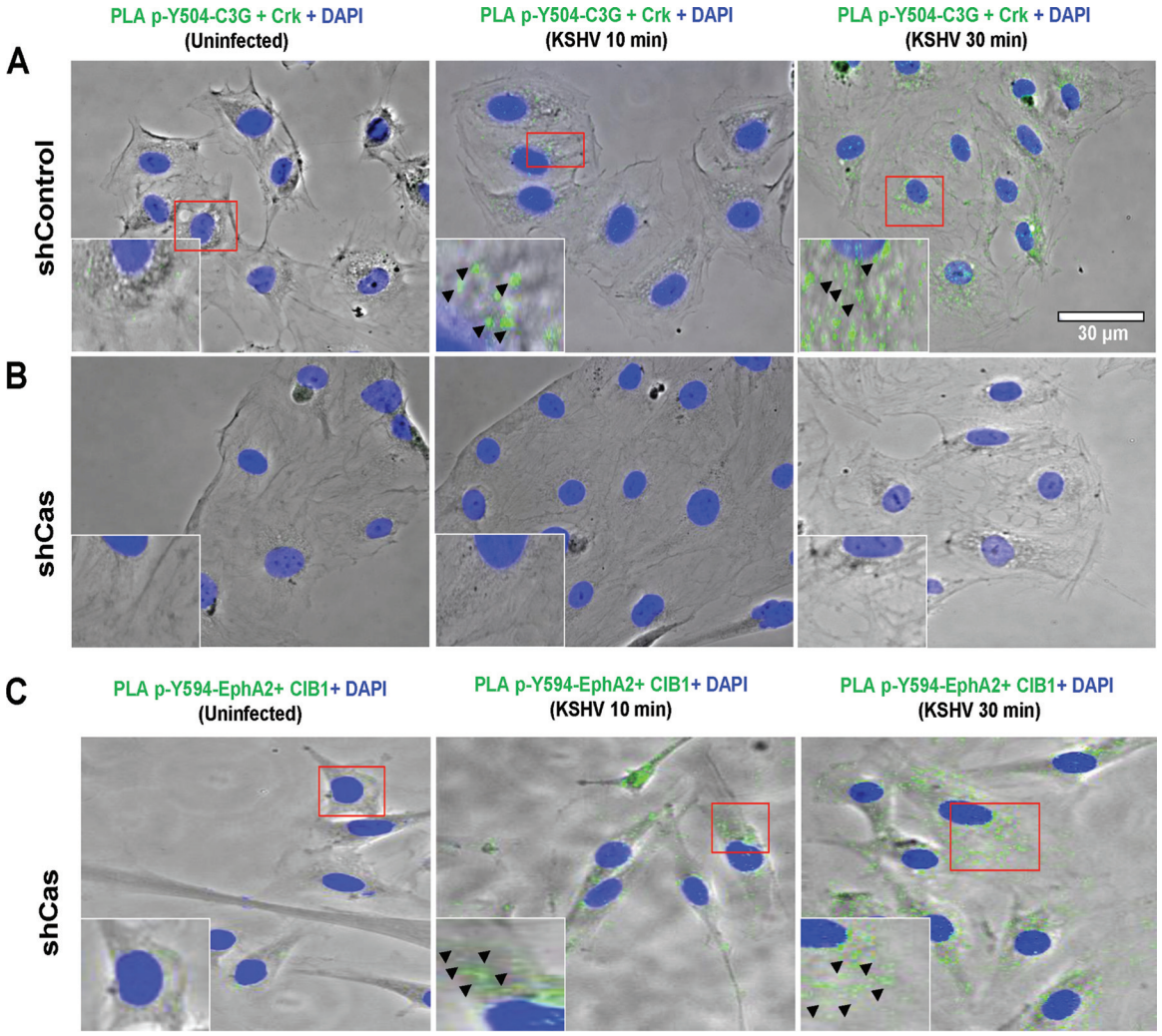

FIG 10 Effect of p130Cas shRNA on KSHV-induced Crk and phospho-C3G association. Control shRNA- (A) or p130Cas shRNA-transduced (B and C) HMVEC-d cells were mock or KSHV infected (20 DNA copies/cell) for the indicated time points. Cells were fixed and processed for proximity ligation assay either with a combination of mouse anti-Crk and rabbit anti-phospho-C3G antibodies (B) or with a combination of rabbit anti-phospho-Y594-EphA2 and mouse anti-CIB1 antibodies (C) and costained with Alexa Fluor 488-conjugated phalloidin and DAPI. Images were merged with the phase contrast images, and the representative immunofluorescence images are shown. Boxed areas in red are enlarged as insets. PLA signals (green dots) in the insets and arrowheads indicate the association of respective molecular combinations. Bar, 30 μm.

data were consistent with our co-IP data (Fig. 6E, iii, lanes 2 to 4). In contrast to control shRNA-transduced cells, p130Cas shRNA transduction completely abolished the PLA signals (green dots) for Crk-phospho C3G association in HMVEC-d cells (Fig. 10B). However, KSHV-induced entry-associated signal amplification events remained unaffected in p130Cas shRNA-transduced HMVEC-d cells as monitored by the PLA method, demonstrating phosho-Y594-EphA2 and CIB1 association (PLA signals in green dots) as early as 10 min p.i., which was sustained until 30 min p.i. (Fig. 10C). These data strongly suggested that Crk-C3G cross talk is a key event downstream to p130Cas and is functionally linked to KSHV productive trafficking.

To decipher the mechanism of p130Cas's role in the KSHV postentry stage of infection further, we examined the association of KSHV with Rab5-positive, Rab7-positive, and Lamp1-positive (early, late, and lysosomal markers, respectively) vesicles in control and p130Cas shRNA-transduced HMVEC-d cells. The respective organelle markers were expressed with a GFP tag using a baculovirus-mediated gene delivery system (Invitrogen) in control and p130Cas shRNA-expressing HMVEC-d cells. Both control and p130Cas shRNA-transduced HMVEC-d cells were checked for Rab5a-GFP, Rab7A-GFP, and Lamp1-GFP expression after ~19 h of incubation with bac-DNA delivery reagent (MOI of 30). Subsequently, shControl cells were infected with envelope-labeled DiI-KSHV for 10 and 30 min, and p130Cas shRNA-transduced cells were infected for 30 min and then processed for immunofluorescence analysis. In control shRNA-transduced cells, as early as 10 min p.i., KSHV (red) was sorted into early endosomes (green) (Fig. 11A, i) and did not colocalize with late endosomes or lysosomal vesicles (Fig. 11B, i, and C, i). At 30 min after infection of shControl HMVEC-d cells, KSHV (red) colocalized with early as well as late endosomes (Fig. 11A, ii, and B, ii), and only a few virus particles colocalized with lysosomes (Fig. 11C, ii). This observation was consistent with our previous findings that KSHV pre-

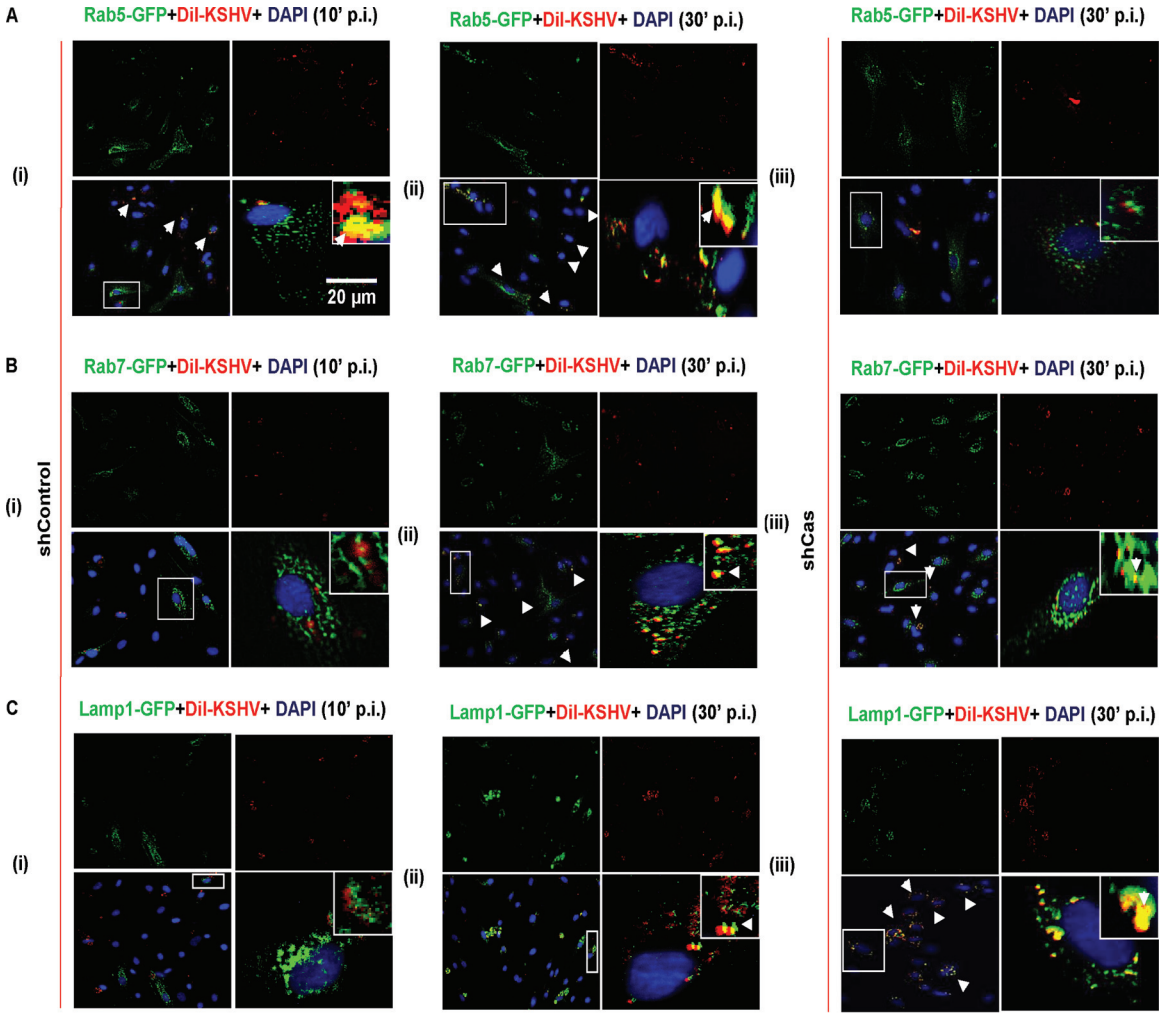

FIG 11 Effect of p130Cas knockdown on the productive trafficking of KSHV in endothelial cells. Control shRNA-transduced (A, i and ii; B, i and ii; and C, i and ii) or p130Cas shRNA-transduced (A, iii; B, iii; and C, iii) HMVEC-d cells were incubated with BacMam 2.0 reagent (baculovirus-mediated gene delivery for Rab5-GFP [A], Rab7-GFP [B], and Lamp1-GFP [C], respectively) for 19 h. Respective organelle-expressing control and p130Cas knockdown HMVEC-d cells were incubated with DiI-KSHV (50 DNA copies/cell) for 10 or 30 min at 37°C. After washing, cells were fixed, permeabilized, and examined by immunofluorescence analysis. Representative deconvoluted images are shown. Higher magnifications (×40) of the boxed areas from the merged panels are shown in the insets. Arrowheads indicate the colocalization of KSHV particles (red) with respective organelles (green). Bar, 20 μm.

dominantly entered via macropinocytosis and was sorted into Rab5- and Rab7-positive vesicles at 10 min p.i., resulting in the productive infection (6, 7, 9). However, a few virus particles colocalizing with lysosome at 30 min p.i. entered via the noninfectious clathrin-mediated endocytic pathway (6, 9). In contrast to control shRNA-transduced cells, in p130Cas shRNA-transduced cells, KSHV particles colocalized significantly with the lysosomes at 30 min p.i. and not with Rab5 or Rab7 (Fig. 11C and A, iii). These results demonstrated that KSHV uptake in p130Cas knockdown cells was rapidly destined to lysosomal degradation, thereby blocking a successful productive infection. These studies were consistent with the live-cell imaging findings in shCas cells (Fig. 8).

These results together with studies shown in Fig. 8, 9, and 10 suggested that the lack of p130Cas scaffolding action enhances the lysosomal degradative pathway possibly by constantly routing KSHV from Rab5- (Fig. 11A, iii) and/or Rab7-positive vesicles (Fig. 11B, iii) to Lamp1-positive lysosomes (Fig. 11C, iii) and clearly demonstrated that p130Cas is a key molecule functionally coupling signal molecules associated with KSHV productive trafficking in HMVEC-d cells.

DISCUSSION

Signal assembly and amplification are the key steps involved at every stage of any physiological or pathological macropinocytosis that includes actin modulation, macropinosome assembly, closure, and trafficking (22, 23, 25, 65–69). KSHV exploits ligand mimicry to induce receptor-ligand clustering on the HMVEC-d cell surface leading into the induction of receptor and downstream intracellular kinases during macropinosome assembly. Most of these entry mediators, possessing SH2 and SH3 domains, are recruited in a simultaneous spatiotemporal manner to the plasma membrane. The present study identified p130Cas as a key molecule in engaging a multiadaptor complex and feed-forward signaling during KSHV macropinocytosis that includes not only

macropinosome assembly but also the trafficking of macropinosome and nuclear delivery of KSHV genome.

The role of major adaptor molecules is well characterized in bacterial pathogenesis. *Yersinia pseudotuberculosis* protein invasin and host cell surface β1 integrin interaction induces FAK and subsequent Src phosphorylation, recruiting p130Cas and downstream Crk for Rac activation, leading to actin-mediated phagocytosis of the pathogens (70). Invasion of *Salmonella enterica* serovar Typhimurium into host cells is coordinated by FAK and p130Cas (37), while *Shigella* is known to use Crk to induce actin polymerization to enter into epithelial cells (34). Host adaptor proteins Gab1 and CrkII play roles in InIB-dependent *Listeria monocytogenes* entry into target cells (33). However, there was a dearth of knowledge regarding the role of these two major adaptor molecules in viral pathogenesis. One study showed that p130Cas, in association with PI3-K, facilitated αVβ5 integrin-mediated adenoviral endocytosis (35); however, the specific route and mechanism of endocytosis were not known. EphA2-mediated cytoskeletal signaling via major cellular scaffold protein p130Cas in other systems is a very well known phenomenon (31). p130Cas is capable of binding to upstream signal molecules such as FAK, Src, and PI3-K as well as many downstream adaptor proteins such as Nck and Crk, etc. (38, 39). Our earlier studies have demonstrated that FAK, Src, PI3-K, and EphA2 molecules play key roles in KSHV entry and in the activation of associated signal pathways (7, 16, 71). We have also recently demonstrated EphA2-mediated signal amplification and cross talk with the actin cytoskeleton during KSHV infection, which is aided by CIB1, a noncanonical adaptor or scaffold molecule (9).

Our comprehensive biochemical and morphological studies highlighted that (i) KSHV macropinosome trafficking is systematized via the scaffold molecule p130Cas, which acts as the main signaling platform for receptor EphA2-downstream multiple adaptor-effector complex formation during post-KSHV-entry trafficking stages, and (ii) p130Cas recruits a variety of canonical adaptors such as c-Cbl, Crk, and C3G, as well as proteins that mimic adaptor functions, such as CIB1, to cumulatively exert a global effect with each single adaptor molecule uniquely positioned to play mechanistic modulation and signaling cross talk roles necessary for the different stages of KSHV macropinocytosis (Fig. 12).

Studies utilizing p130Cas shRNA demonstrated that although KSHV entered the cells efficiently, it did not proceed toward a productive infection but instead was routed toward lysosomal degradation (Fig. 8, 9, and 11), which is an exciting observation. Our previous studies demonstrated that the absence of adaptor c-Cbl detoured KSHV toward lysosomal degradation, and we initially reasoned that this could be due to switching of pathways via selective signaling in KSHV entry receptor integrins (6). However, p130Cas shRNA knockdown did not abrogate KSHV-induced bleb-mediated macropinocytosis but promoted trafficking of internalized KSHV very rapidly to lysosomes, which could occur by inhibiting downstream Crk association with phospho-C3G molecules (Fig. 10). These important data not only designated a new scaffold function for p130Cas but also opened up a new phenomenon of steady versus rapid sorting of viruses and associated signaling in postentry cargo trafficking toward the nucleus or lysosome for KSHV in the absence of cellular p130Cas. That knockdown of p130Cas affects Crk-C3G cross talk and directly or indirectly regulates cargo trafficking is another new finding of this study. C3G is shown to be a guanine nucleotide exchange factor that catalyzes GDP-GTP exchange to activate cellular GTPases. C3G-activated GTPases are primarily associated with actin cytoskeletal motility under physiological or pathological conditions associated with human malignancies (44). C3G action is explored in a variety of receptor-associated signaling events that include integrins, B and T cell receptors, insulin, epidermal growth factor receptor (EGFR), nerve growth factor receptor (NGFR), and gamma interferon (72–79). C3G is functionally tied to intracellular vesicle transport, particularly in transportation of GLUT4 downstream to insulin receptor signaling (80), interaction with E-cadherin vesicle trafficking in regulating cellular junctional disassembly, and activation of Rab11-positive recycling endosomes (81, 82). However, involvement of the Crk-C3G axis in sorting productive pathways for virus trafficking is a completely new addition to C3G function. Further studies are essential to decipher mechanistic details of C3G-GEF action in KSHV cargo-containing vesicle fusion and maturation from early to late endosomes and/or subverting late endosomes to lysosomes.

DiI labels the envelope of the virus, and a significantly higher level of perinuclear staining of KSHV was observed in shCas HMVEC-d cells but not in control shRNA-transduced HMVEC-d cells (Fig. 8B and 9B), which is consistent with the characteristic perinuclear trans-Golgi staining of active lysosomes (59–64). This phenomenon also strongly corroborated with the experimental evidence in Fig. 11 which demonstrated that in shCas HMVEC-d cells, the virus particles accumulated in lysosomes possibly by constant routing of KSHV from Rab5- (Fig. 11A, iii) and/or Rab7-positive vesicles (Fig. 11B, iii) to Lamp1-positive lysosomes (Fig. 11C, iii). The lack of p130Cas scaffolding action did not hamper the biogenesis of lysosome biogenesis (Fig. 11C, iii). Whether enhanced lysosomal targeting is due to a defect in pH-dependent deenvelopment of the virus is beyond the scope of the present study and needs further investigation.

Our biochemical fractionation and coimmunoprecipitation studies revealed that p130Cas translocated to the lipid raft regions of HMVEC-d cells and assembled a signalosome that consisted of the receptor EphA2, E3 ubiquitin ligase c-Cbl, signal amplifier CIB1, adaptor Crk, and effector GEF as early as 5 min p.i. that was sustained for 30 min p.i. Owing to its scaffolding property, p130Cas facilitated KSHV-induced molecular signal complex cross talk presumably by regulating spatiotemporal proximity of molecules, which collectively culminated in functional determination of internalized KSHV destination to intracellular vesicles. Exploring endosomal localization kinetics of each upstream and downstream signal molecule placed in the p130Cas signal axis during KSHV intracellular vesicle transport would shed further light on p130Cas scaffold function during primary KSHV infection.

Our earlier electron microscopic studies have demonstrated that KSHV induces membrane protrusions as early as 5 and 10 min p.i. (9) of HMVEC-d cells, which is followed by a very rapid internalization of virus into large irregularly shaped macropinocytic vesicles and that subsequent fusion of virion envelope with the endocytic vesicle membrane releases the capsid from the macropinosome into the cytosol. The stages during KSHV entry and postentry are highly overlapping. Thus, not all bound viruses are internalized at the same time. As a result, infectious particles may be observed inside the macropinosome, whereas some can still be found at the periphery of the cell. In our earlier confocal and electron microscopic studies, at 5 min p.i., we have also observed a few KSHV capsid particles in the cytoplasm, which were

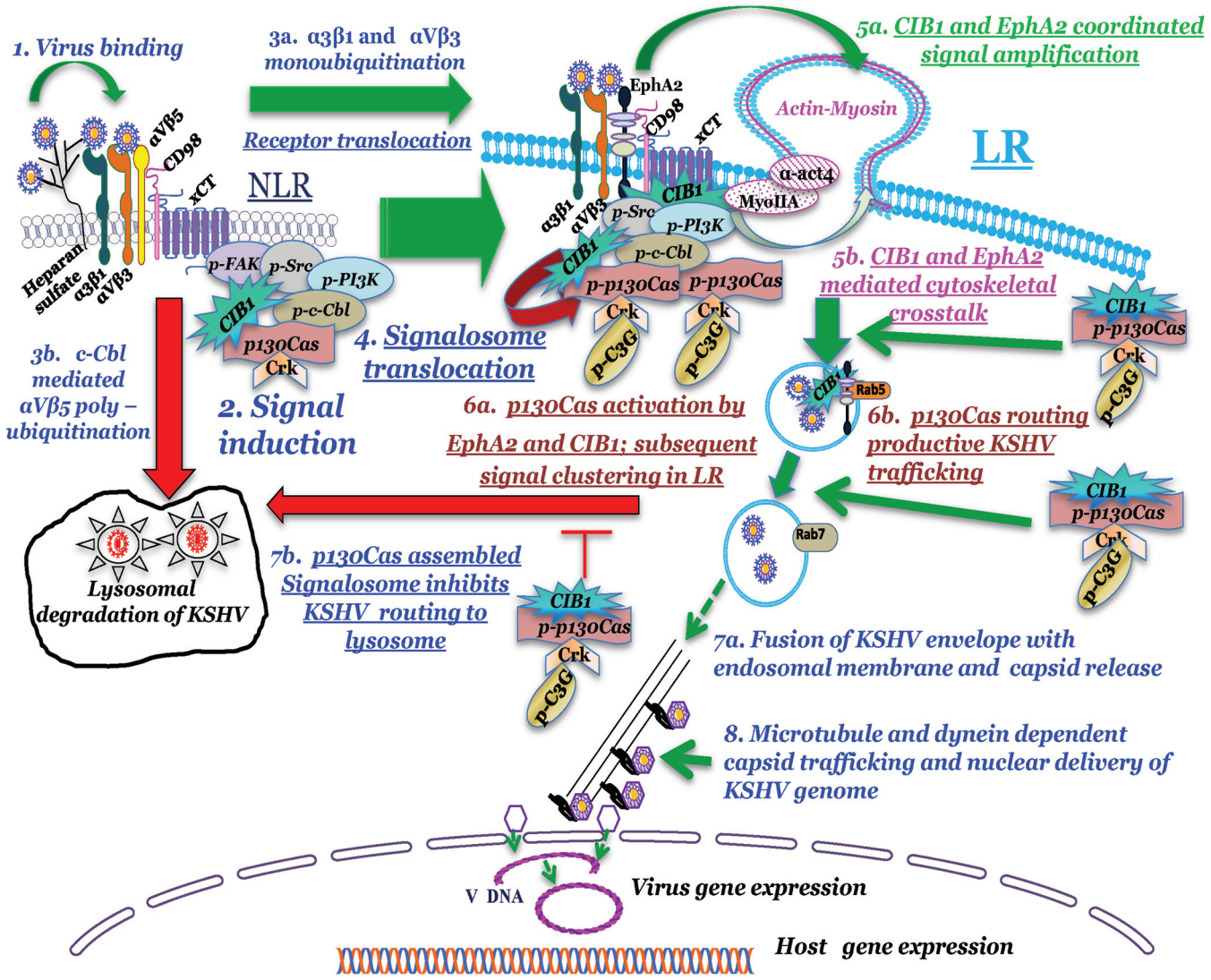

FIG 12 Model depicting the role of scaffold protein p130Cas during KSHV primary infection in HMVEC-d cells. KSHV binding (1) to the NLR region-localized integrin receptors (α3β1 and αVβ3) activates downstream signal molecules (2) and promotes NLR recruitment of CIB1, p130Cas, and Crk molecules along with other KSHV entry mediators. KSHV-bound selective integrin receptor (α3β1 and αVβ3) translocation to LR (3a) and LR-associated entry receptor EphA2 activation promote signal clustering, which enhances LR recruitment and/or LR translocation of CIB1, p130Cas, and Crk molecules (4 and 5). EphA2 and CIB1 synergize to facilitate KSHV entry and signal amplification, which promote simultaneous phosphorylation of downstream scaffold molecule p130Cas (6a). p130Cas assembles EphA2-CIB1-c-Cbl-Crk and activated GEF C3G molecules to accelerate postentry stages of macropinosome trafficking (6b), which eventually leads to release of KSHV capsid from the endosome (7a) and nuclear delivery of the KSHV genome (8). p130Cas-assembled signalosome guides KSHV to deliver its genome into the infected HMVEC-d cell nucleus and establish successful productive primary infection. p130Cas-regulated Crk and phospho-C3G association directly or indirectly uncouples KSHV detouring toward lysosomal degradation (7b). Our studies have clearly demonstrated that p130Cas is a key molecule functionally coupling signal molecules associated with KSHV productive trafficking in HMVEC-d cells.

probably released from the endocytic vesicles (9, 13). These studies have demonstrated that KSHV entry is a very fast and dynamic process and that the event dynamicity probably depends on the number of virus particles infecting a single HMVEC-d cell.

Overall, our studies reveal for the first time that p130Cas plays critical roles in recruiting multiple adaptor molecules, such as EphA2-CIB1-c-Cbl-Crk-C3G, resulting in a unique signal axis that regulates the stages of pathological (viral) macropinocytosis and thus facilitates herpesvirus trafficking. Hence, simultaneous targeting of KSHV entry receptors and p130Cas to block KSHV entry as well as abolish productive trafficking is an attractive strategy to control KSHV infection and resulting malignancies such as Kaposi's sarcoma.

ACKNOWLEDGMENTS

This study was supported in part by Public Health Service grants CA 075911 and CA 168472 and the Rosalind Franklin University of Medicine and Science H. M. Bligh Cancer Research Fund to B.C.

We thank Keith Philibert for critically reading the manuscript and Patricia Loomis (Confocal Microscopy Core Facility, Rosalind Franklin University of Medicine and Science) for assisting with microscopic studies.

REFERENCES

1. **Ganem D.** 2007. Kaposi's sarcoma-associated herpesvirus, p 2875–2888. *In* Knipe DM, Howley PM, Griffin DE, Lamb RA, Martin MA, Roizman B, Strauss SE (ed), Fields virology, 5th ed, vol 2. Lippincott Williams & Wilkins, Philadelphia, PA.
2. **Cesarman E, Chang Y, Moore PS, Said JW, Knowles DM.** 1995. Kaposi's sarcoma-associated herpesvirus-like DNA sequences in AIDS-related body-cavity-based lymphomas. N. Engl. J. Med. **332:**1186–1191. http://dx.doi.org/10.1056/NEJM199505043321802.
3. **Chang Y, Cesarman E, Pessin MS, Lee F, Culpepper J, Knowles DM, Moore PS.** 1994. Identification of herpesvirus-like DNA sequences in AIDS-associated Kaposi's sarcoma. Science **266:**1865–1869. http://dx.doi.org/10.1126/science.7997879.
4. **Chandran B.** 2010. Early events in Kaposi's sarcoma-associated herpesvirus infection of target cells. J. Virol. **84:**2188–2199. http://dx.doi.org/10.1128/JVI.01334-09.
5. **Chakraborty S, Veettil MV, Chandran B.** 2012. Kaposi's sarcoma associated herpesvirus entry into target cells. Front. Microbiol. **3:**6. http://dx.doi.org/10.3389/fmicb.2012.00006.
6. **Chakraborty S, ValiyaVeettil M, Sadagopan S, Paudel N, Chandran B.** 2011. c-Cbl-mediated selective virus-receptor translocations into lipid rafts regulate productive Kaposi's sarcoma-associated herpesvirus infection in endothelial cells. J. Virol. **85:**12410–12430. http://dx.doi.org/10.1128/JVI.05953-11.
7. **Chakraborty S, Veettil MV, Bottero V, Chandran B.** 2012. Kaposi's sarcoma-associated herpesvirus interacts with EphrinA2 receptor to amplify signaling essential for productive infection. Proc. Natl. Acad. Sci. U. S. A. **109:**E1163–E1172. http://dx.doi.org/10.1073/pnas.1119592109.
8. **Valiya Veettil M, Sadagopan S, Kerur N, Chakraborty S, Chandran B.** 2010. Interaction of c-Cbl with myosin IIA regulates Bleb associated macropinocytosis of Kaposi's sarcoma-associated herpesvirus. PLoS Pathog. **6:**e1001238. http://dx.doi.org/10.1371/journal.ppat.1001238.
9. **Bandyopadhyay C, Valiya-Veettil M, Dutta D, Chakraborty S, Chandran B.** 2014. CIB1 synergizes with EphrinA2 to regulate Kaposi's sarcoma-associated herpesvirus macropinocytic entry in human microvascular dermal endothelial cells. PLoS Pathog. **10:**e1003941. http://dx.doi.org/10.1371/journal.ppat.1003941.
10. **Dutta D, Chakraborty S, Bandyopadhyay C, Valiya Veettil M, Ansari MA, Singh VV, Chandran B.** 2013. EphrinA2 regulates clathrin mediated KSHV endocytosis in fibroblast cells by coordinating integrin-associated signaling and c-Cbl directed polyubiquitination. PLoS Pathog. **9:**e1003510. http://dx.doi.org/10.1371/journal.ppat.1003510.
11. **Kerur N, Veettil MV, Sharma-Walia N, Sadagopan S, Bottero V, Paul AG, Chandran B.** 2010. Characterization of entry and infection of monocytic THP-1 cells by Kaposi's sarcoma associated herpesvirus (KSHV): role of heparan sulfate, DC-SIGN, integrins and signaling. Virology **406:**103–116. http://dx.doi.org/10.1016/j.virol.2010.07.012.
12. **Raghu H, Sharma-Walia N, Veettil MV, Sadagopan S, Caballero A, Sivakumar R, Varga L, Bottero V, Chandran B.** 2007. Lipid rafts of primary endothelial cells are essential for Kaposi's sarcoma-associated herpesvirus/human herpesvirus 8-induced phosphatidylinositol 3-kinase and RhoA-GTPases critical for microtubule dynamics and nuclear delivery of viral DNA but dispensable for binding and entry. J. Virol. **81:**7941–7959. http://dx.doi.org/10.1128/JVI.02848-06.
13. **Raghu H, Sharma-Walia N, Veettil MV, Sadagopan S, Chandran B.** 2009. Kaposi's sarcoma-associated herpesvirus utilizes an actin polymerization-dependent macropinocytic pathway to enter human dermal microvascular endothelial and human umbilical vein endothelial cells. J. Virol. **83:**4895–4911. http://dx.doi.org/10.1128/JVI.02498-08.
14. **Veettil MV, Sharma-Walia N, Sadagopan S, Raghu H, Sivakumar R, Naranatt PP, Chandran B.** 2006. RhoA-GTPase facilitates entry of Kaposi's sarcoma-associated herpesvirus into adherent target cells in a Src-dependent manner. J. Virol. **80:**11432–11446. http://dx.doi.org/10.1128/JVI.01342-06.
15. **Krishnan HH, Sharma-Walia N, Streblow DN, Naranatt PP, Chandran B.** 2006. Focal adhesion kinase is critical for entry of Kaposi's sarcoma-associated herpesvirus into target cells. J. Virol. **80:**1167–1180. http://dx.doi.org/10.1128/JVI.80.3.1167-1180.2006.
16. **Sharma-Walia N, Naranatt PP, Krishnan HH, Zeng L, Chandran B.** 2004. Kaposi's sarcoma-associated herpesvirus/human herpesvirus 8 envelope glycoprotein gB induces the integrin-dependent focal adhesion kinase-Src-phosphatidylinositol 3-kinase-rho GTPase signal pathways and cytoskeletal rearrangements. J. Virol. **78:**4207–4223. http://dx.doi.org/10.1128/JVI.78.8.4207-4223.2004.
17. **Veettil MV, Sadagopan S, Sharma-Walia N, Wang FZ, Raghu H, Varga L, Chandran B.** 2008. Kaposi's sarcoma-associated herpesvirus forms a multimolecular complex of integrins (alphaVbeta5, alphaVbeta3, and alpha3beta1) and CD98-xCT during infection of human dermal microvascular endothelial cells, and CD98-xCT is essential for the postentry stage of infection. J. Virol. **82:**12126–12144. http://dx.doi.org/10.1128/JVI.01146-08.
18. **Shukla D, Spear PG.** 2001. Herpesviruses and heparan sulfate: an intimate relationship in aid of viral entry. J. Clin. Invest. **108:**503–510. http://dx.doi.org/10.1172/JCI13799.
19. **Hahn AS, Desrosiers RC.** 2013. Rhesus monkey rhadinovirus uses eph family receptors for entry into B cells and endothelial cells but not fibroblasts. PLoS Pathog. **9:**e1003360. http://dx.doi.org/10.1371/journal.ppat.1003360.
20. **Hahn AS, Kaufmann JK, Wies E, Naschberger E, Panteleev-Ivlev J, Schmidt K, Holzer A, Schmidt M, Chen J, Konig S, Ensser A, Myoung J, Brockmeyer NH, Sturzl M, Fleckenstein B, Neipel F.** 2012. The ephrin receptor tyrosine kinase A2 is a cellular receptor for Kaposi's sarcoma-associated herpesvirus. Nat. Med. **18:**961–966. http://dx.doi.org/10.1038/nm.2805.
21. **Chakraborty S, ValiyaVeettil M, Sadagopan S, Paudel N, Chandran B.** 2011. c-Cbl-mediated selective virus-receptor translocations into lipid rafts regulate productive Kaposi's sarcoma-associated herpesvirus infection in endothelial cells. J. Virol. **85:**12410–12430. http://dx.doi.org/10.1128/JVI.05953-11.
22. **Jones AT.** 2007. Macropinocytosis: searching for an endocytic identity and role in the uptake of cell penetrating peptides. J. Cell. Mol. Med. **11:**670–684. http://dx.doi.org/10.1111/j.1582-4934.2007.00062.x.
23. **Kerr MC, Teasdale RD.** 2009. Defining macropinocytosis. Traffic **10:**364–371. http://dx.doi.org/10.1111/j.1600-0854.2009.00878.x.
24. **Marsh M, Helenius A.** 2006. Virus entry: open sesame. Cell **124:**729–740. http://dx.doi.org/10.1016/j.cell.2006.02.007.
25. **Mercer J, Helenius A.** 2012. Gulping rather than sipping: macropinocytosis as a way of virus entry. Curr. Opin. Microbiol. **15:**490–499. http://dx.doi.org/10.1016/j.mib.2012.05.016.
26. **Mercer J, Helenius A.** 2008. Vaccinia virus uses macropinocytosis and apoptotic mimicry to enter host cells. Science **320:**531–535. http://dx.doi.org/10.1126/science.1155164.
27. **Mercer J, Schelhaas M, Helenius A.** 2010. Virus entry by endocytosis. Annu. Rev. Biochem. **79:**803–833. http://dx.doi.org/10.1146/annurev-biochem-060208-104626.
28. **Gobeil LA, Lodge R, Tremblay MJ.** 2013. Macropinocytosis-like HIV-1 internalization in macrophages is CCR5 dependent and leads to efficient but delayed degradation in endosomal compartments. J. Virol. **87:**735–745. http://dx.doi.org/10.1128/JVI.01802-12.
29. **Coyne CB, Shen L, Turner JR, Bergelson JM.** 2007. Coxsackievirus entry across epithelial tight junctions requires occludin and the small GTPases Rab34 and Rab5. Cell Host Microbe **2:**181–192. http://dx.doi.org/10.1016/j.chom.2007.07.003.
30. **Krieger SE, Kim C, Zhang L, Marjomaki V, Bergelson JM.** 2013. Echovirus 1 entry into polarized Caco-2 cells depends on dynamin, cholesterol, and cellular factors associated with macropinocytosis. J. Virol. **87:**8884–8895. http://dx.doi.org/10.1128/JVI.03415-12.
31. **Carter N, Nakamoto T, Hirai H, Hunter T.** 2002. EphrinA1-induced cytoskeletal re-organization requires FAK and p130(cas). Nat. Cell Biol. **4:**565–573. http://dx.doi.org/10.1038/ncb823.
32. **Dikic I, Szymkiewicz I, Soubeyran P.** 2003. Cbl signaling networks in the regulation of cell function. Cell. Mol. Life Sci. **60:**1805–1827. http://dx.doi.org/10.1007/s00018-003-3029-4.
33. **Sun H, Shen Y, Dokainish H, Holgado-Madruga M, Wong A, Ireton K.** 2005. Host adaptor proteins Gab1 and CrkII promote InlB-dependent entry of Listeria monocytogenes. Cell. Microbiol. **7:**443–457. http://dx.doi.org/10.1111/j.1462-5822.2004.00475.x.
34. **Bougneres L, Girardin SE, Weed SA, Karginov AV, Olivo-Marin JC, Parsons JT, Sansonetti PJ, Van Nhieu GT.** 2004. Cortactin and Crk

cooperate to trigger actin polymerization during Shigella invasion of epithelial cells. J. Cell Biol. **166:**225–235. http://dx.doi.org/10.1083/jcb.200402073.
35. **Li E, Stupack DG, Brown SL, Klemke R, Schlaepfer DD, Nemerow GR.** 2000. Association of p130CAS with phosphatidylinositol-3-OH kinase mediates adenovirus cell entry. J. Biol. Chem. **275:**14729–14735. http://dx.doi.org/10.1074/jbc.275.19.14729.
36. **Dokainish H, Gavicherla B, Shen Y, Ireton K.** 2007. The carboxyl-terminal SH3 domain of the mammalian adaptor CrkII promotes internalization of Listeria monocytogenes through activation of host phosphoinositide 3-kinase. Cell. Microbiol. **9:**2497–2516. http://dx.doi.org/10.1111/j.1462-5822.2007.00976.x.
37. **Shi J, Casanova JE.** 2006. Invasion of host cells by Salmonella typhimurium requires focal adhesion kinase and p130Cas. Mol. Biol. Cell **17:**4698–4708. http://dx.doi.org/10.1091/mbc.E06-06-0492.
38. **Barrett A, Pellet-Many C, Zachary IC, Evans IM, Frankel P.** 2013. p130Cas: a key signalling node in health and disease. Cell. Signal. **25:**766–777. http://dx.doi.org/10.1016/j.cellsig.2012.12.019.
39. **Defilippi P, Di Stefano P, Cabodi S.** 2006. p130Cas: a versatile scaffold in signaling networks. Trends Cell Biol. **16:**257–263. http://dx.doi.org/10.1016/j.tcb.2006.03.003.
40. **Ruest PJ, Shin NY, Polte TR, Zhang X, Hanks SK.** 2001. Mechanisms of CAS substrate domain tyrosine phosphorylation by FAK and Src. Mol. Cell. Biol. **21:**7641–7652. http://dx.doi.org/10.1128/MCB.21.22.7641-7652.2001.
41. **Birge RB, Kalodimos C, Inagaki F, Tanaka S.** 2009. Crk and CrkL adaptor proteins: networks for physiological and pathological signaling. Cell Commun. Signal. **7:**13. http://dx.doi.org/10.1186/1478-811X-7-13.
42. **Mayer BJ, Hanafusa H.** 1990. Association of the v-crk oncogene product with phosphotyrosine-containing proteins and protein kinase activity. Proc. Natl. Acad. Sci. U. S. A. **87:**2638–2642. http://dx.doi.org/10.1073/pnas.87.7.2638.
43. **Mayer BJ, Hamaguchi M, Hanafusa H.** 1988. A novel viral oncogene with structural similarity to phospholipase C. Nature **332:**272–275. http://dx.doi.org/10.1038/332272a0.
44. **Radha V, Mitra A, Dayma K, Sasikumar K.** 2011. Signalling to actin: role of C3G, a multitasking guanine-nucleotide-exchange factor. Biosci. Rep. **31:**231–244. http://dx.doi.org/10.1042/BSR20100094.
45. **Escalante M, Courtney J, Chin WG, Teng KK, Kim JI, Fajardo JE, Mayer BJ, Hempstead BL, Birge RB.** 2000. Phosphorylation of c-Crk II on the negative regulatory Tyr222 mediates nerve growth factor-induced cell spreading and morphogenesis. J. Biol. Chem. **275:**24787–24797. http://dx.doi.org/10.1074/jbc.M000711200.
46. **Shin NY, Dise RS, Schneider-Mergener J, Ritchie MD, Kilkenny DM, Hanks SK.** 2004. Subsets of the major tyrosine phosphorylation sites in Crk-associated substrate (CAS) are sufficient to promote cell migration. J. Biol. Chem. **279:**38331–38337. http://dx.doi.org/10.1074/jbc.M404675200.
47. **Kumar S, Fajardo JE, Birge RB, Sriram G.** 2014. Crk at the quarter century mark: perspectives in signaling and cancer. J. Cell. Biochem. **115:**819–825. http://dx.doi.org/10.1002/jcb.24749.
48. **Akula SM, Pramod NP, Wang FZ, Chandran B.** 2002. Integrin alpha3beta1 (CD 49c/29) is a cellular receptor for Kaposi's sarcoma-associated herpesvirus (KSHV/HHV-8) entry into the target cells. Cell **108:**407–419. http://dx.doi.org/10.1016/S0092-8674(02)00628-1.
49. **Krishnan HH, Naranatt PP, Smith MS, Zeng L, Bloomer C, Chandran B.** 2004. Concurrent expression of latent and a limited number of lytic genes with immune modulation and antiapoptotic function by Kaposi's sarcoma-associated herpesvirus early during infection of primary endothelial and fibroblast cells and subsequent decline of lytic gene expression. J. Virol. **78:**3601–3620. http://dx.doi.org/10.1128/JVI.78.7.3601-3620.2004.
50. **Le Blanc I, Luyet PP, Pons V, Ferguson C, Emans N, Petiot A, Mayran N, Demaurex N, Faure J, Sadoul R, Parton RG, Gruenberg J.** 2005. Endosome-to-cytosol transport of viral nucleocapsids. Nat. Cell Biol. **7:**653–664. http://dx.doi.org/10.1038/ncb1269.
51. **Zhu FX, Li X, Zhou F, Gao SJ, Yuan Y.** 2006. Functional characterization of Kaposi's sarcoma-associated herpesvirus ORF45 by bacterial artificial chromosome-based mutagenesis. J. Virol. **80:**12187–12196. http://dx.doi.org/10.1128/JVI.01275-06.
52. **Sadagopan S, Sharma-Walia N, Veettil MV, Bottero V, Levine R, Vart RJ, Chandran B.** 2009. Kaposi's sarcoma-associated herpesvirus upregulates angiogenin during infection of human dermal microvascular endothelial cells, which induces 45S rRNA synthesis, antiapoptosis, cell proliferation, migration, and angiogenesis. J. Virol. **83:**3342–3364. http://dx.doi.org/10.1128/JVI.02052-08.
53. **Wang FZ, Akula SM, Sharma-Walia N, Zeng L, Chandran B.** 2003. Human herpesvirus 8 envelope glycoprotein B mediates cell adhesion via its RGD sequence. J. Virol. **77:**3131–3147. http://dx.doi.org/10.1128/JVI.77.5.3131-3147.2003.
54. **Weibrecht I, Leuchowius KJ, Clausson CM, Conze T, Jarvius M, Howell WM, Kamali-Moghaddam M, Soderberg O.** 2010. Proximity ligation assays: a recent addition to the proteomics toolbox. Expert Rev. Proteomics **7:**401–409. http://dx.doi.org/10.1586/epr.10.10.
55. **Dutta S, Bandyopadhyay C, Bottero V, Veettil MV, Wilson L, Pins MR, Johnson KE, Warshall C, Chandran B.** 2014. Angiogenin interacts with the plasminogen activation system at the cell surface of breast cancer cells to regulate plasmin formation and cell migration. Mol. Oncol. **8:**483–507. http://dx.doi.org/10.1016/j.molonc.2013.12.017.
56. **Song KS, Li S, Okamoto T, Quilliam LA, Sargiacomo M, Lisanti MP.** 1996. Co-purification and direct interaction of Ras with caveolin, an integral membrane protein of caveolae microdomains. Detergent-free purification of caveolae microdomains. J. Biol. Chem. **271:**9690–9697.
57. **Naranatt PP, Krishnan HH, Smith MS, Chandran B.** 2005. Kaposi's sarcoma-associated herpesvirus modulates microtubule dynamics via RhoA-GTP-diaphanous 2 signaling and utilizes the dynein motors to deliver its DNA to the nucleus. J. Virol. **79:**1191–1206. http://dx.doi.org/10.1128/JVI.79.2.1191-1206.2005.
58. **Brabek J, Constancio SS, Siesser PF, Shin NY, Pozzi A, Hanks SK.** 2005. Crk-associated substrate tyrosine phosphorylation sites are critical for invasion and metastasis of SRC-transformed cells. Mol. Cancer Res. **3:**307–315. http://dx.doi.org/10.1158/1541-7786.MCR-05-0015.
59. **Matteoni R, Kreis TE.** 1987. Translocation and clustering of endosomes and lysosomes depends on microtubules. J. Cell Biol. **105:**1253–1265. http://dx.doi.org/10.1083/jcb.105.3.1253.
60. **Beguinot L, Lyall RM, Willingham MC, Pastan I.** 1984. Down-regulation of the epidermal growth factor receptor in KB cells is due to receptor internalization and subsequent degradation in lysosomes. Proc. Natl. Acad. Sci. U. S. A. **81:**2384–2388. http://dx.doi.org/10.1073/pnas.81.8.2384.
61. **Dodson MW, Zhang T, Jiang C, Chen S, Guo M.** 2012. Roles of the Drosophila LRRK2 homolog in Rab7-dependent lysosomal positioning. Hum. Mol. Genet. **21:**1350–1363. http://dx.doi.org/10.1093/hmg/ddr573.
62. **Bucci C, Thomsen P, Nicoziani P, McCarthy J, van Deurs B.** 2000. Rab7: a key to lysosome biogenesis. Mol. Biol. Cell **11:**467–480. http://dx.doi.org/10.1091/mbc.11.2.467.
63. **Falcon-Perez JM, Nazarian R, Sabatti C, Dell'Angelica EC.** 2005. Distribution and dynamics of Lamp1-containing endocytic organelles in fibroblasts deficient in BLOC-3. J. Cell Sci. **118:**5243–5255. http://dx.doi.org/10.1242/jcs.02633.
64. **Feng Y, Press B, Wandinger-Ness A.** 1995. Rab 7: an important regulator of late endocytic membrane traffic. J. Cell Biol. **131:**1435–1452. http://dx.doi.org/10.1083/jcb.131.6.1435.
65. **Akhtar J, Shukla D.** 2009. Viral entry mechanisms: cellular and viral mediators of herpes simplex virus entry. FEBS J. **276:**7228–7236. http://dx.doi.org/10.1111/j.1742-4658.2009.07402.x.
66. **Amyere M, Payrastre B, Krause U, Van Der Smissen P, Veithen A, Courtoy PJ.** 2000. Constitutive macropinocytosis in oncogene-transformed fibroblasts depends on sequential permanent activation of phosphoinositide 3-kinase and phospholipase C. Mol. Biol. Cell **11:**3453–3467. http://dx.doi.org/10.1091/mbc.11.10.3453.
67. **Araki N, Johnson MT, Swanson JA.** 1996. A role for phosphoinositide 3-kinase in the completion of macropinocytosis and phagocytosis by macrophages. J. Cell Biol. **135:**1249–1260. http://dx.doi.org/10.1083/jcb.135.5.1249.
68. **Kasahara K, Nakayama Y, Sato I, Ikeda K, Hoshino M, Endo T, Yamaguchi N.** 2007. Role of Src-family kinases in formation and trafficking of macropinosomes. J. Cell. Physiol. **211:**220–232. http://dx.doi.org/10.1002/jcp.20931.
69. **Mettlen M, Platek A, Van Der Smissen P, Carpentier S, Amyere M, Lanzetti L, de Diesbach P, Tyteca D, Courtoy PJ.** 2006. Src triggers circular ruffling and macropinocytosis at the apical surface of polarized MDCK cells. Traffic **7:**589–603. http://dx.doi.org/10.1111/j.1600-0854.2006.00412.x.
70. **Gustavsson A, Yuan M, Fallman M.** 2004. Temporal dissection of beta1-integrin signaling indicates a role for p130Cas-Crk in filopodia

formation. J. Biol. Chem. **279:**22893–22901. http://dx.doi.org/10.1074/jbc.M309693200.

71. **Naranatt PP, Akula SM, Zien CA, Krishnan HH, Chandran B.** 2003. Kaposi's sarcoma-associated herpesvirus induces the phosphatidylinositol 3-kinase-PKC-zeta-MEK-ERK signaling pathway in target cells early during infection: implications for infectivity. J. Virol. **77:**1524–1539. http://dx.doi.org/10.1128/JVI.77.2.1524-1539.2003.
72. **Uemura N, Griffin JD.** 1999. The adapter protein Crkl links Cbl to C3G after integrin ligation and enhances cell migration. J. Biol. Chem. **274:**37525–37532. http://dx.doi.org/10.1074/jbc.274.53.37525.
73. **Takino T, Tamura M, Miyamori H, Araki M, Matsumoto K, Sato H, Yamada KM.** 2003. Tyrosine phosphorylation of the CrkII adaptor protein modulates cell migration. J. Cell Sci. **116:**3145–3155. http://dx.doi.org/10.1242/jcs.00632.
74. **Tanaka S, Ouchi T, Hanafusa H.** 1997. Downstream of Crk adaptor signaling pathway: activation of Jun kinase by v-Crk through the guanine nucleotide exchange protein C3G. Proc. Natl. Acad. Sci. U. S. A. **94:**2356–2361. http://dx.doi.org/10.1073/pnas.94.6.2356.
75. **Reedquist KA, Fukazawa T, Panchamoorthy G, Langdon WY, Shoelson SE, Druker BJ, Band H.** 1996. Stimulation through the T cell receptor induces Cbl association with Crk proteins and the guanine nucleotide exchange protein C3G. J. Biol. Chem. **271:**8435–8442. http://dx.doi.org/10.1074/jbc.271.14.8435.
76. **Smit L, van der Horst G, Borst J.** 1996. Sos, Vav, and C3G participate in B cell receptor-induced signaling pathways and differentially associate with Shc-Grb2, Crk, and Crk-L adaptors. J. Biol. Chem. **271:**8564–8569. http://dx.doi.org/10.1074/jbc.271.15.8564.
77. **Alsayed Y, Uddin S, Ahmad S, Majchrzak B, Druker BJ, Fish EN, Platanias LC.** 2000. IFN-gamma activates the C3G/Rap1 signaling pathway. J. Immunol. **164:**1800–1806. http://dx.doi.org/10.4049/jimmunol.164.4.1800.
78. **Nosaka Y, Arai A, Miyasaka N, Miura O.** 1999. CrkL mediates Ras-dependent activation of the Raf/ERK pathway through the guanine nucleotide exchange factor C3G in hematopoietic cells stimulated with erythropoietin or interleukin-3. J. Biol. Chem. **274:**30154–30162. http://dx.doi.org/10.1074/jbc.274.42.30154.
79. **Du J, Alsayed YM, Xin F, Ackerman SJ, Platanias LC.** 2000. Engagement of the CrkL adapter in interleukin-5 signaling in eosinophils. J. Biol. Chem. **275:**33167–33175. http://dx.doi.org/10.1074/jbc.M003655200.
80. **Chiang SH, Baumann CA, Kanzaki M, Thurmond DC, Watson RT, Neudauer CL, Macara IG, Pessin JE, Saltiel AR.** 2001. Insulin-stimulated GLUT4 translocation requires the CAP-dependent activation of TC10. Nature **410:**944–948. http://dx.doi.org/10.1038/35073608.
81. **Balzac F, Avolio M, Degani S, Kaverina I, Torti M, Silengo L, Small JV, Retta SF.** 2005. E-cadherin endocytosis regulates the activity of Rap1: a traffic light GTPase at the crossroads between cadherin and integrin function. J. Cell Sci. **118:**4765–4783. http://dx.doi.org/10.1242/jcs.02584.
82. **Kanzaki M, Watson RT, Hou JC, Stamnes M, Saltiel AR, Pessin JE.** 2002. Small GTP-binding protein TC10 differentially regulates two distinct populations of filamentous actin in 3T3L1 adipocytes. Mol. Biol. Cell **13:**2334–2346. http://dx.doi.org/10.1091/mbc.01-10-0490.